DEPARTMENT OF CLINICAL MEDICINE

FACULTY OF MEDICINE AND HEALTH SCIENCES

MACQUARIE UNIVERSITY

Application of photoluminescent nanomaterials for diagnosis and therapy of bladder cancer

Dmitry Polikarpov

This thesis is submitted as a partial fulfilment to the requirements for the degree of Master of Research in Medicine and Health Sciences

Submission date: 10th October 2016

Table of Contents

ABSTRACT VII
STATEMENT OF ORIGINALITY VIII
ACKNOWLEDGMENTS IX
ABBREVIATIONS XI
AIM AND HYPOTHESIS OF THIS RESEARCH PROJECT XII
STRUCTURE OF THIS THESIS XIII

CHAPTER 1: REVIEW OF CURRENT STATE OF BLADDER CANCER AND PHOTODYNAMIC DIAGNOSIS AND THERAPY 1

1.1. Introduction 1

1.2. Current state of bladder cancer diagnosis and therapy 2

1.2.1. Epidemiology, etiology and presentation of bladder cancer 2
1.2.2. Classification of non-muscle invasive bladder cancer 3
1.2.3. Patients with resistant non-muscle invasive bladder cancer 4
1.2.4. Reasons for bladder cancer recurrence and progression 6

1.3. Existing and emerging techniques for photodynamic diagnosis and therapy of bladder cancer 7

1.3.1. Influence of photodynamic diagnosis and therapy on recurrence and progression of bladder cancer 7
1.3.2. Existing photodynamic agents for application on bladder cancer 8
1.3.3. Limitations of conventional photodynamic agents 12
1.3.4. Contemporary approach to photodynamic diagnosis and therapy 14

1.4. Conclusions of the review of current state of bladder cancer and research objectives of this study 20

1.4.1. Conclusions of the literature review 20
1.4.2. Approach 21
1.4.3. Research objectives 22

CHAPTER 2: PRODUCTION AND CHARACTERISATION OF TARGETED UPCONVERSION PHOTOLUMINESCENT NANOCONJUGATES 24

2.1. Introduction 24

2.2. Materials and methodologies applied in the production, characterisation and conjugation of upconversion nanoparticles 25

2.2.1. Reagents for production of upconversion nanoconjugates 25
2.2.2. Equipment used in characterisation of upconversion nanoparticles 26
2.2.3. Methodology of synthesis of upconversion nanoparticles 26
2.2.4. Conjugation of upconversion nanoparticles with LPG linkers 28
2.2.5. Production of the targeted upconversion nanoconjugates 30

2.3. Results of the synthesis and conjugation of upconversion nanoparticles 32

2.3.1. Upconversion nanoparticles amenable for conjugation with biomolecules 32
2.3.2. Upconversion nanoparticles conjugated with LPG 36
2.3.3. Targeted photoluminescent upconversion nanoconjugates 36

2.4. Conclusions 39

CHAPTER 3: CULTURING AND CHARACTERISATION OF UROTHELIAL CARCINOMA CELL LINES T24 AND C3 40

3.1. Introduction 40

3.2. Materials and methods applied in the culturing of T24 and C3 urothelial carcinoma cell lines 40

3.2.1. Reagents used for cell culturing 40
3.2.2. Equipment used for cell culturing and investigation 41
3.2.3. Origin of T24 and C3 urothelial carcinoma cell lines 42
3.2.4. *In vitro* culturing of T24 and C3 urothelial carcinoma cell lines 42

3.3. Results of the investigation and optimisation of the culturing of T24 and C3 urothelial carcinoma cells 43

3.3.1. Characteristics of T24 and C3 urothelial carcinoma cell lines 43

3.3.2. Effects of coverslip coating on adhesion and growth of urothelial carcinoma cells T24 and C3 46

3.3.3. Optimal seeding density and fixation time point of T24 cells 47

3.4. Conclusions 48

CHAPTER 4: TARGETED LABELLING OF UROTHELIAL CARCINOMA CELLS BY PHOTOLUMINESCENT NANOCONJUGATES 49

4.1. Introduction 49

4.2. Materials and methods applied in the investigation of targeted labelling of urothelial carcinoma cells 49

4.2.1. Equipment for the analysis of targeted labelling of urothelial carcinoma cells 49

4.2.2. Seeding of T24 and C3 cells to cell culture plates for the study of targeted labelling 50

4.2.3. Methodology of the incubation of T24 and C3 urothelial carcinoma cells with nanoconjugates 51

4.2.4. Methodology of confocal laser scanning microscopy of cells labelled by nanoconjugates 52

4.2.5. Methodology of the analysis of targeted labelling 53

4.3. Results of the experimental study of targeted labelling of urothelial carcinoma cells 55

4.3.1. Results of visual analysis of confocal microscopy images 55

4.3.2. Results of visual quantification of labelled cells 59

4.3.3. Results of the analysis of the intensity of photoluminescence of cells in different groups 61

4.4. Conclusions 63

CHAPTER 5: DISCUSSION, CONCLUSIONS AND FUTURE DIRECTIONS 64

5.1. Discussion of the techniques applied in this study 64

5.2. Significance of the results and potential applications 66

5.2.1. Potential application in bladder cancer diagnosis 67

5.2.2. Potential application in bladder cancer therapy 68

5.3. Limitations of this research project 69

5.4. Conclusions 71

5.5. Future directions 71

REFERENCES 73

Abstract

Approximately three-quarters of bladder cancer patients initially present with a non-muscle invasive tumour, which is usually resected. Transurethral resection can be followed by adjuvant chemo- and immune-therapy. However, in up to 50% of patients, aggressive flat lesions remain intact and progress into muscle-invasive disease, potentially leading to cystectomy and a less favourable outcome.

This project addresses the development of novel biohybrid nanocomplexes representing upconversion nanoparticles coupled to antibodies termed targeted upconversion photoluminescent nanoconjugates for photodynamic diagnosis and therapy of bladder cancer. The unique photophysical properties of upconversion nanoparticles allow optical imaging at the centimetre-depth in biological tissue, which is demanded for a number of applications in urology. Coupled to specific antibodies, these nanoconjugates selectively bind to urothelial carcinoma cells and make them visible by emitting visible photoluminescence upon excitation with deeply-penetrating near-infrared light. This photoluminescence can be used for tumour detection and fluorescence-guided resection. In addition, photoluminescent nanoconjugates can carry photosensitiser drugs to cancer cells followed by their photoactivation for targeted photodynamic therapy.

In this study, upconversion nanoparticles were synthesised, coated with a silica layer and linked to anti-Glypican-1 antibody MIL38. Incubation with urothelial carcinoma cells with high expression of Glypican-1 (T24) and control cells with low expression of Glypican-1 (C3) demonstrated specific binding of these nanoconjugates to cells expressing the target antigen. This result highlights potential of this technology for further studies of their application in the diagnosis and therapy of bladder cancer.

Statement of originality

I certify that the work in this thesis entitled "Application of photoluminescent nanomaterials for diagnosis and therapy of bladder cancer" has not previously been submitted for a degree nor has it been submitted as part of requirements for a degree to any other university or institution other than Macquarie University. I also certify that the thesis is an original piece of research and it has been written by me. Any help and assistance that I have received in my research work and the preparation of the thesis itself have been appropriately acknowledged. In addition, I certify that all information sources and literature used are indicated in this thesis. Ethics Committee approval was not required for this research project.

Dmitry Polikarpov (Student ID: 44813643)

10th October 2016

Acknowledgments

First of all, I would like to thank my principal supervisor Professor David Gillatt and co-supervisors Associate Professor Andrei Zvyagin and Professor Gilles Guillemin for their assistance in planning and realisation of this research project. They were an invaluable source of support and encouragement. Without their dedication to medical research and extensive experience in urological oncology, optical biomedical imaging and sensing, biomarkers and cell biology, this project would not be possible.

I am very grateful to Research Fellow Dr Tharani Sabaretnam for her constant support and guidance through the experimental design and laboratory work.

I would like to thank biomarker research company Minomic International Ltd., its Chief Executive Officer Dr Bradley Walsh, Head of Research and Development Dr Douglas Campbell and Research Scientist Padraig McCauley Winter for their guidance and support in this research project. I am also thankful to them for providing me with urothelial carcinoma cell lines and antibody MIL38.

My thanks also go to ARC Centre of Excellence for Nanoscale BioPhotonics (CNBP) and its Deputy Director Professor Ewa Goldys and Research Officer and Laboratory Manager Dr Ayad Anwer for their advices and training of the basics of cell culturing and confocal microscopy. It also goes to CNBP members from the Department of Chemistry and Biomolecular Sciences Associate Professor Anwar Sunna, and Research Fellow Dr Andrew Care for their guidance, training and providing me with LPG linker and antibody CRY104.

I am grateful to PhD candidate Ms Liuen (Olivia) Liang for her support, training and help with the production, conjugation and characterisation of upconversion nanoparticles.

I am also thankful to Optical Bioimaging and Sensing group, MQ BioFocus Research Centre, Macquarie University Motor Neurone Disease Research Centre and Neuroinflammation group.

I would like to thank: Macquarie University for International Research Training Pathway scholarship and for the opportunity to do this project; HDR Student Administration Officer at the Faculty of Medicine and Health Sciences Viviana Bong for her assistance throughout this year; Research Operations Manager Louise Marr, Laboratory Operations Officer Lucy Lu and Laboratory Operations Coordinator Tamara Leo for their help and for excellent working conditions in the laboratory of the Faculty of Medicine and Health Sciences; and HDR Learning Skills Advisor Dr Jennifer Rowland for improving my medical research writing and presentation skills.

Finally, I would never be able to finish my research project and prepare this thesis without constant support of my family. I would like to express my sincere gratitude to my father Mikhail and mother Dina for their support, encouragement, understanding and for making me who I am today. I am grateful to my lovely wife Aleksandra for bringing so much comfort and happiness into my life. I would also like to thank my sister Dasha and her husband Peter for welcoming me and making me feel at home in Australia.

Abbreviations

5-ALA – 5-Aminolevulinic acid

BCG – Bacille Calmette-Guerin

Ce6-PVP – Chlorin e6-polyvinylpyrrolidone

CIS – Carcinoma *in situ*

Er – Erbium

F – Fluoride

Fab – antigen-binding fragment of immunoglobulin G

Fc – crystallisable fragment of immunoglobulin G

Ig-G – Immunoglobulin G

HAL – Hexaminolevulinic acid

HpD – Haematoporphirin derivative

LPG – Linker-Protein-G

MIBC – Muscle-invasive bladder cancer

Na – Sodium

NIR – Near-infrared

NMIBC – Non-muscle-invasive bladder cancer

PBS – Phosphate-buffered saline

PFA – Paraformaldehyde

PDD – Photodynamic diagnosis

PDT – Photodynamic therapy

PpIX – Protoporphyrin IX

RPMI – Roswell Park Memorial Institute

TURBT – Transurethral resection of bladder tumour

UCNP – Upconversion nanoparticle

Y – Yttrium

Yr – Ytterbium

Aim and hypothesis of this research project

Bladder cancer is the fourth most common cancer in men, eleventh in women[1] and one of the most expensive tumours to treat[2]. Despite the considerable progress in biotechnology and medicine over the past few decades, the recurrence and progression rates of bladder cancer remain significant and emphasise a need for novel methods of bladder cancer diagnosis and therapy.

This project aims to investigate means of targeted labelling of urothelial carcinoma cells by photoluminescent nanoparticles functionalised with specific antibodies. This represents the first stage of this study aimed at development of a novel photoluminescent nanoconjugate for early detection, fluorescence-guided resection and deeply-penetrating targeted photodynamic therapy (PDT) of non-muscle-invasive bladder cancer (NMIBC). This *in vitro* study represents a proof-of-concept and the first step in the development of diagnostic and therapeutic agents based on upconversion nanoparticles and enables their optimisation for further studies *in vivo*.

This study hypothesises that upconversion photoluminescent nanoparticles can be functionalised by a monoclonal antibody, selectively label urothelial carcinoma cells expressing a specific antigen and emit visible photoluminescence.

Structure of this thesis

This thesis includes five chapters, which give concise description of this research project aimed at the investigation of application of photoluminescent nanomaterials for diagnosis and therapy of bladder cancer.

The first chapter identifies patients with NMIBC who need novel methods of diagnosis and therapy. Then it reviews possible causes and mechanisms of bladder cancer recurrence and progression together with existing methods of photodynamic diagnosis (PDD) and PDT of bladder cancer. It also suggests the ways to overcome resistance of bladder cancer and gives information about prospective contemporary methods. Finally, this chapter describes our approach to the problem of resistant non-muscle-invasive disease and outlines main objectives of this study.

The second chapter describes production of upconversion nanoparticles and their conjugation with antibodies. Then it details characteristics of these targeted photoluminescent nanoconjugates.

The third chapter gives information about the morphology, adhesion and growth of urothelial carcinoma cell cultures, which were studied in this project and outlines the process of their preparation for investigation of targeted labelling.

The fourth chapter describes the investigation of targeted labelling of urothelial carcinoma cells by targeted nanoconjugates. It also highlights the role of a monoclonal antibody MIL38 in targeted binding of the nanoconjugates to urothelial carcinoma cells.

The final chapter compares the results of this research project with the existing methods and describes its significance and potential applications. This chapter then outlines the limitations of this study, conclusions and intended future directions for further development of this research project.

Chapter 1: Review of current state of bladder cancer and photodynamic diagnosis and therapy

1.1. Introduction

This chapter provides a background for this research project. The first part gives information about the epidemiology, etiology, presentation and classification of bladder cancer. The next section contains a more detailed characterisation of non-muscle-invasive disease, its classification, diagnosis, therapy and issues associated with the management of patients with this type of cancer who do not respond to standard treatment. It also identifies a number of possible reasons for unsuccessful treatment of bladder cancer and mechanisms of its recurrence and progression.

This chapter then provides a review of PDD and PDT of bladder cancer and describes its mechanisms and overall effects of these techniques on cancer recurrence and progression. Moreover, this chapter reviews conventional photodynamic methodologies, investigated preclinically or applied clinically for diagnosis and therapy of patients diagnosed with bladder cancer. Then, it identifies limitations inherent to existing photodynamic techniques and ways to overcome them. After that, this chapter reviews novel methods, such as photoluminescent nanomaterials, and highlights the reasons why upconversion photoluminescent nanoparticles have great potential in this field.

The last part of this chapter summarises findings of this review and describes our approach and the research objectives of this study.

1.2. Current state of bladder cancer diagnosis and therapy

1.2.1. Epidemiology, etiology and presentation of bladder cancer

Bladder cancer is the ninth most common cancer worldwide[3]. In 2012, bladder cancer was diagnosed in 430,000 patients and caused 156,000 deaths[3]. Due to a high risk of recurrence and progression of bladder cancer, every patient needs long-term surveillance, which includes regular cystoscopy, sometimes followed by a biopsy of suspicious lesions or resections of recurring tumours. This surveillance, as well as a number of other aspects, make bladder cancer one of the most expensive tumours to treat on a per patient basis[4-7].

Genetic factors and exposure to carcinogens are the main etiological factors of bladder cancer[8]. Alterations of genes responsible for urine concentration and neutralisation of some carcinogens are among those discovered to increase risk of bladder cancer[9-11]. Major external sources of carcinogens causing urothelial cancer are tobacco smoking and occupational exposure. Tobacco smoke is the main cause of urothelial cancer. It contains carcinogens that are excreted through the urinary system and directly contact all parts of the urinary tract, increasing risk of bladder cancer fourfold compared to that of non-smokers[12-14]. Approximately 20% of bladder cancers are estimated to be caused by occupational exposure to carcinogens, such as aromatic amines and chlorinated or polycyclic aromatic hydrocarbons. Most often, these compounds affect workers in tobacco factories, dye workers and chimney sweeps[8,15]. Another common factor causing bladder cancer is infection of the urinary tract with a parasite trematode *Schistosoma haematobium*. This infection leads to squamous cell carcinoma of the urinary bladder and is observed predominantly in northern Africa[8].

About 80% of bladder tumours manifest with painless haematuria, while others can present with irritative urinary symptoms or pain of different localisation, which is usually associated with the later stages of this disease[16-20]. The most reliable method of diagnosing bladder cancer is cystoscopy, an endoscopic examination of the inside of the urinary bladder through the urethra. Any suspicious lesions detected during cystoscopy are removed by a transurethral resection of bladder tumour (TURBT) procedure. Resected samples are sent for a histological analysis, in order to confirm the diagnosis and determine grade and invasiveness of the disease[16-18,21,22]. High-grade tumours consist of undifferentiated cells and are more likely to recur or progress than better-differentiated low-grade tumours[16,23]. Depending on the invasiveness, bladder cancer can be muscle invasive (MIBC) if it invades a muscle layer of the urinary bladder or NMIBC, if it is confined to the urothelium and subepithelial connective tissue (*lamina propria*)[16,21].

1.2.2. Classification of non-muscle invasive bladder cancer

Approximately 75% of patients are initially diagnosed with NMIBC, which may present as three types of tumour: Ta – papillary tumour, confined to the urothelium; T1 – tumour invaded into the subepithelial connective tissue; or CIS (Carcinoma in-situ) – flat, low differentiated tumour in the urothelium (**Figure 1**)[18,21,22]. Depending on the risk of recurrence and progression, these tumours can be classified as low, intermediate and high risk[21]. Patients with well-differentiated Ta tumours have low or intermediate risk and should be treated by transurethral resection and immediate single adjuvant chemotherapy instillation, which, in some cases, should be followed by a 1-year maintenance chemotherapy or Bacille Calmette-Guerin (BCG) immunotherapy. In contrast, CIS, T1 and poorly differentiated Ta tumours have high risk of recurrence and progression, therefore, patients with such tumours require up to 3 years of BCG immunotherapy

following TURBT. In addition, while T1 and Ta tumours are more likely to reoccur, rather than progress, CIS tumours tend to invade and progress to MIBC more often, resulting in the necessity of radical cystectomy and worsening of survival prognosis for such patients[24]. Another issue associated with CIS tumours is that they are extremely challenging to detect during cystoscopy as they can look like an inflamed or completely normal urothelium of the bladder wall.

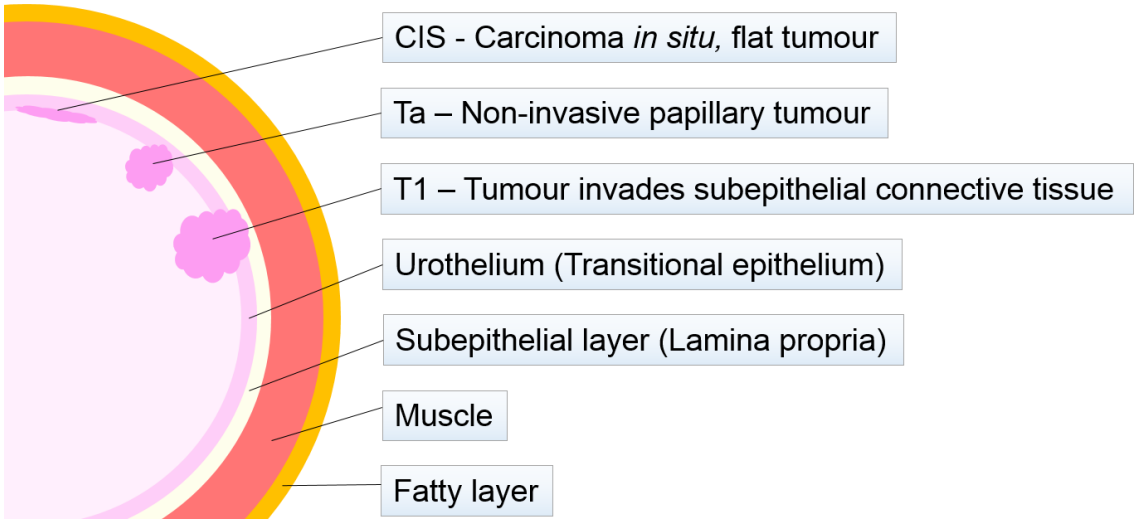

Figure 1. Layers of the bladder wall and stages of non-muscle invasive bladder cancer.

1.2.3. Patients with resistant non-muscle invasive bladder cancer

Despite the treatment modalities mentioned above, up to 50% of the patients diagnosed with NMIBC have recurrence or progress and eventually require surgical removal of their urinary bladder (termed radical cystectomy) as multiple TURBT and long-term BCG immunotherapy are not effective[18,25,26].

In general, every recurrence or progression after a course of BCG immunotherapy is considered as BCG failure. However, due to the diversity of BCG failures, they were divided into four groups[27]. The first group includes BCG refractory patients whose

condition remained unchanged or worsened after a 6-month course of BCG treatment. The second group is BCG resistant patients. In contrast with the first group, they respond to BCG, however, this response is slow and characterised by the reduction of tumour only after 3 months and absence of the tumour after 6 months of BCG immunotherapy. The third group is BCG relapsing patients, who respond well at first but relapse after 12 months or later. The forth group is BCG intolerant. These patients are not suitable for BCG therapy because of its individual toxicity or side effects.

More recent classification by European Association of Urology categorised BCG intolerance separately from BCG failures[23]. The first of the three groups of BCG failures in their classification is detection of MIBC after a course of immunotherapy for a NMIBC. The second group is BCG-refractory tumours and included high-grade tumours remaining intact after 3 months of BCG therapy, CIS tumours remaining intact after 6 months of BCG therapy and new high-grade tumours that appear during BCG therapy. The third group is a recurrence of high-grade tumours after a course of BCG, despite initial response.

One of the purposes of the BCG failures classification is to define for which patients further BCG immunotherapy will not be effective. Currently, radical cystectomy is a gold standard for the management of patients with NMIBC who failed BCG and should not be postponed without a reason[16,18,21,22]. Raj *et al*. have shown an increase of the survival in patients with early radical cystectomy after BCG failure compared to repeated transurethral resection followed by a course of immunotherapy[28]. However, radical cystectomy is a highly invasive procedure, associated with many risks and significant morbidity[29]. As a result, a significant number of patients are unfit or unwilling to undergo radical surgery[30,31]. A range of therapies is currently available for these

patients. However, these therapies are less effective than radical cystectomy and may cause excessive adverse side effects[32,33].

1.2.4. Reasons for bladder cancer recurrence and progression

A number of known reasons can cause recurrence or progression of bladder cancer despite active therapy. In general, it is usually caused by the incomplete initial treatment. It can be incomplete resection, which may lead to the development of remaining tumours and tumour cells, or ineffective adjuvant therapy, which may lead to reimplantation of cancer cells[34].

Incomplete TURBT may lead to understaging of the disease. If the resected sample does not include obturator muscle, a patient diagnosed with NMIBC can in fact have MIBC. This understaging was found by the pathology study in a significant proportion of patients (40%), who were initially diagnosed with NMIBC and had a radical cystectomy[35]. The second known reason for the recurrence and progression is initial incomplete resection of tumour margins[35].

It was found that the site of initial tumour and surrounding tissues are the most common locations of recurrence (33% - 67 %), which means that a new tumour had most likely grown from the remaining non-resected part of the original lesion[36,37]. Another type of incomplete resection is missing tumours that are not visible during initial TURBT, such as CIS. This tumour can be extremely hard to detect as it can look like an inflammation or be completely unnoticeable[23]. Missed CIS lesions can progress rapidly and lead to an aggressive MIBC and cystectomy.

The implantation of tumour cells disturbed during TURBT is another major cause of recurrence and progression. Immediate chemo or immune adjuvant therapies are aimed at the avoidance of this implantation, however, sometimes they are not effective enough.

1.3. Existing and emerging techniques for photodynamic diagnosis and therapy of bladder cancer

1.3.1. Influence of photodynamic diagnosis and therapy on recurrence and progression of bladder cancer

Photodynamic diagnosis (PDD) is a method based on the accumulation of photosensitisers in cancerous lesions and their photoluminescence under the excitation by light of a specific wavelength. In urology, this method is used in cystoscopy and such cystoscopy is called fluorescence cystoscopy. In fluorescence cystoscopy, a photosensitiser can be administered either intravesically or intravenously and the excitation radiation is delivered via a transurethral endoscope to excite the photosensitiser[38]. In comparison with conventional white-light cystoscopy, the fluorescence cystoscopy was found to be superior for detection of bladder tumours (92% versus 71%), especially, CIS[16,23,39]. Fluorescence can also guide a surgeon taking a biopsy and resecting the tumour.

Another application of photosensitisers in urology is PDT of NMIBC. In PDT, a photosensitiser accumulates in cancerous cells and produces reactive oxygen species under illumination by the excitation light. Despite several relatively successful clinical trials, PDT is not widely used in the therapy of bladder cancer. Preclinical studies of novel photodynamic drugs are still ongoing.

Both, PDD and PDT are very promising platforms in diagnosis and therapy of bladder cancer capable to reduce the recurrence and progression. While fluorescence cystoscopy can help surgeons detect a tumour at the early stage, fluorescence-guided resection can help them avoid incompleteness and understaging, showing the inconspicuous margins. PDT, as an adjuvant therapy can ablate remaining cancerous cells, avoiding their implantation. Another benefit of PDT is its integration of three mechanisms of action on tumour cells. In addition to the direct cytotoxic effect of reactive oxygen species on tumour cells and damage of the tumour vasculature, it induces an inflammatory reaction, which may play a significant role in bladder cancer therapy[40]. Therefore, application of PDD and PDT in bladder cancer therapy has seen a significant development over the past decades. A number of photodynamic agents studied preclinically or applied clinically in diagnosis and therapy of bladder cancer are described in the following paragraphs.

1.3.2. Existing photodynamic agents for application on bladder cancer

1.3.2.1. Haematoporphirin derivative

The first photosensitiser used for photodynamic therapy of bladder cancer was haematoporphirin derivative (HpD) Porfimer sodium. This agent showed preferable accumulation in cancer cells and caused mitochondrial damage. *In vivo* studies demonstrated that 2-3 days after administration, the agent accumulated in cancerous cells evading the majority of normal cells, leading to the reduction of the effects on healthy bladder wall[41,42]. Porfimer sodium was effective for some patients, reducing the recurrence and progression rates in a number of clinical trials carried out from 1983 to 2003[43-49]. However, accumulation of this photosensitiser in normal cells was also relatively high and long-lasting. Consequently, patients suffered from side effects,

including skin photosensitivity, irritative bladder symptoms and possibly other complications for several weeks[45,46,49-54].

Experimental use of HpD for diagnosis of bladder cancer in the fluorescence cystoscopy was reported from 1976[44,48,55-57]. Application of Porfimer sodium for the diagnosis of bladder cancer was also associated with the same side effects[58]. The presence of these adverse side effects urged further development of novel agents for bladder cancer photodynamic diagnosis and therapy.

1.3.2.2. Photodynamic agents based on aminolevulinic acid

The study of Porfimer sodium was followed by the development of 5-Aminolevulinic acid (5-ALA). Five-ALA participates in the production of haem in living cells. The pivotal product in this process is a strong endogenous photosensitiser protoporphyrin IX (PpIX). Administered orally or intravesically, 5-ALA can cause excessive production of PpIX only in cancer cells due to the metabolic difference, causing their photoluminescence and death under illumination of the bladder wall. Compared to the derivatives of haematoporphirin, 5-ALA demonstrated higher efficiency and exhibited fewer side effects[59]. However, since 5-ALA is a hydrophilic amino acid, its cellular uptake was relatively low and biodistribution was heterogeneous[60-62]. Another disadvantage of this agent was the possibility of haemodynamic instability in patients after its systemic intravenous administration.

In order to enhance the cellular uptake of a photosensitiser and to optimise its biodistribution, a hexil ester of 5-ALA, hexaminolevulinic acid (HAL) was synthesised. Hexaminolevulinic acid is characterised by the higher lipophilicity. This quality allows deeper penetration into tissues, better accumulation in tumours and better sensitivity. It

has shown up to a 25-fold increase in PpIX levels in malignant cells compared to normal cells and a more homogeneous distribution across the tumour. High concentrations of PpIX in cancer cells can be achieved faster than with 5-ALA[63]. Another benefit of HAL is a significant increase in fluorescence compared to the agents used previously[64]. Phase 1 clinical study of PDT with HAL was performed by Bader *et al*. in 2013[65]. HAL was administered intravesically and resulted in transient irritative symptoms with no systemic adverse effects.

Application of HAL was much more significant in bladder cancer diagnosis. In 2003, HAL was reported to be more effective than 5-ALA, causing stronger fluorescence and better tumour-to-healthy cell accumulation ratio[66]. Numerous clinical studies have taken place over the following years. In 2013, a meta-analysis of these studies by Burger *et al*. has confirmed improved detection and recurrence after the fluorescence cystoscopy with HAL in comparison with conventional white-light cystoscopy[67]. Long-term risk of progression was analysed by Gakis and Fahmu in 2016. They also confirmed better outcomes after the fluorescence cystoscopy with HAL in comparison with white-light cystoscopy[68]. HAL-assisted fluorescence cystoscopy has been recommended in the latest guidelines on bladder cancer from European Association of Urology, American Urological Association and a number of other international and national panels[16,23,39,69]. Sensitivity of HAL was found to be significantly higher than that of white-light cystoscopy, detecting 92% and 71% of tumours, respectively. However, the specificity of HAL fluorescence cystoscopy was found to be 63%, which was lower than those of white-light, reaching 81%[70]. One of the possible reasons was speculated to be the accumulation of HAL in inflamed tissues and immune cells, as its selectivity was based only on the metabolic differences between normal and cancer cells[23,71].

1.3.2.3. Chlorine-based photodynamic agents

After a number of successful preclinical studies, novel chlorin-based photosensitiser, chlorin e6-polyvinylpyrrolidone (Ce6-PVP) was of a high interest, as a potential photodynamic agent for bladder cancer[72,73]. The first clinical trial of this agent was performed by Lee *et al*. in 2010[74]. The study included only five patients, four of whom received Ce6-PVP intravesically and one patient had an intravenous administration. Of all these patients, four had complete response at three-month follow-up. All patients reported the presence of mild irritative symptoms lasting for less than a week after the procedure. The patient who received Ce6-PVP intravenously had an enterovesical fistula 16 month after the PDT. The other patients had no systemic side effects after intravesical instillation of Ce6-PVP, due to the absence of the systemic uptake, which was confirmed by the emission spectroscopy of blood serum. Even though this study has shown that treatment with Ce6-PVP is effective in some patients, the cohort was relatively small and further studies with more patients and longer surveillance are required to validate the safety and therapeutic performance of this agent.

Photodynamic therapy with Porfimer sodium, 5-ALA and HAL requires the use of red 630-635-nm light whose penetration into tissues of the human body is limited to 6-8 mm. In contrast, a complex natural photosensitiser Radachlorin can be irradiated by 662-nm light and penetrates up to 10 mm[74]. This photosensitiser has a high cellular uptake and homogenous distribution[75]. Radachlorin has a short clearance time of 24-48 hours, which produced no long-term adverse side effects[75]. Furthermore, in a clinical trial Radachlorin has shown better response rates than the other agents[76]. However, adverse side effects were still relatively common among the patients. Another limitation is that

even 10 mm is not enough to eliminate residual bladder tumours thoroughly, as its size can easily reach more than 10 mm[77].

1.3.2.4. Hypericin

Hypericin is a naturally occurring compound sourced from a number of plants of the genus *Hypericum*. Preferential accumulation of Hypericin in bladder tumours in comparison with healthy urothelium was demonstrated *in vivo* by Kamuhabva, *et al*. and caused increasing interest in the use of this agent for bladder cancer PDD and PDT[78]. Whereas the application of Hypericin for PDT was limited to preclinical studies[78,79], its use for PDD attracted more attention. A number of clinical studies demonstrated a potential of Hypericin as a drug for fluorescence cystoscopy[78-83]. The main advantages of Hypericin in comparison with 5-ALA and HAL were reported to be the higher specificity and lower photobleaching, allowing the use of the lower drug dose and achieving photoluminescence for the longer excitation time exposures[38,84]. Straub, *et al*. have recently reported their results of phase IIA clinical study and announced a multicentre phase IIB study, where the sensitivity and specificity of polyvinylpyrrolidone-hypericin fluorescence cystoscopy will be assessed[84].

1.3.3. Limitations of conventional photodynamic agents

Despite the remarkable success of PDD and PDT of bladder cancer and recommendation of PDD by major international panels, several studies had controversial results with inconsistent effects of fluorescence cystoscopy on progression[70,85,86]. Even though a gradual development allowed an increase of the efficacy and reduction of side effects of the existing photodynamic agents, they have a number of limitations[51,87,88].

Conventional photosensitisers demonstrate good sensitivity, detecting almost all tumours, while their specificity is lower than those of white-light cystoscopy. The mechanism of their specific accumulation in tumours, which is based only on slight differences in the metabolism between cancerous and normal cells, is likely to account for this poor specificity [89]. As a result, conventional 5-aminolevulinic acid based photodynamic agents suffer from the excessive accumulation in inflamed regions of the bladder wall and can result in unwanted skin accumulation, if applied intravenously, leading to phototoxicity and limitation of its clinical applicability[90].

Another problem of the conventional photodynamic agents is difficulty of their modification and optimisation. It is a major issue in the light of the findings of the phenotypic diversity and high variability of cancer characteristics[91-94]. Consequently, their efficacy can be inconsistent in different patients.

Conventional PDD and PDT can be applied only superficially, as their depth is limited by the penetration depth of visible light through bladder tissues. Even though the latest photosensitisers can be excited by far red light with the better penetration, its penetration is limited to 10 mm, which is not enough, as some bladder tumours can reach more than 10 mm in size[76].

Finally, conventional photodynamic agents cannot carry other drugs and combine multiple modalities of action on cancer cells, such as photothermal action, chemotherapy, radiotherapy or immunotherapy[90].

1.3.4. Contemporary approach to photodynamic diagnosis and therapy

1.3.4.1. Nanomaterials as novel multifunctional photodynamic agents

Development of new methods and approaches for the diagnosis and therapy of malignant tumours is one of the most dynamic and actively developing areas of biomedicine. Over the past few decades, great progress has been made in studying the genetic characteristics[91,95-97], molecular basis[98] and metabolic pathways[99] of tumours. This knowledge allowed the establishment of a model of a highly effective contemporary medical approach that should: (1) be based on the individual molecular profile of the disease in each patient, (2) involve various mechanisms of action on cancer cells and (3) allow monitoring of the treatment progress. These tasks can be carried by one of the most promising methods in oncology, "theranostics", which is based on the use of multifunctional agents for simultaneous molecular diagnostic and specific targeted therapeutic action on tumour cells with monitoring of treatment response[100].

Targeted theranostic agents need to be characterised by high stability and low toxicity. Also, they must be amenable for bioconjugation with other molecules, as theranostic agents have to be assembled from targeting, diagnostic and therapeutic modules. The majority of such multifunctional agents are based on a variety of nanocompounds, such as iron oxide magnetic nanoparticles[101-104], carbon nanotubes[105], gold nanoparticles[106] and silica nanoparticles[107,108]. All of these nanomaterials have their own advantages and disadvantages and can be optimal for specific applications.

Due to the convenience of transurethral endoscopic access, PDT may be the best platform for theranostics of bladder cancer[90]. Novel multifunctional photodynamic nanoconjugates should be able to allow early detection of tumours, guide a surgeon during

resection and deliver targeted PDT to kill remaining tumours and disturbed cancer cells. Another prerequisite for these nanoconjugates is the ability to be optimised for the highest possible efficacy in every patient, depending on characteristics of their tumour. A multifunctional agent able to be used for both photodynamic diagnosis and therapy of bladder cancer must consist of a targeting part, that can bind to bladder tumour, a part that can produce bright luminescence and a part that can cause death of cancer cells.

1.3.4.2. Photoluminescent nanomaterials, upconversion nanoparticles

Over the past few decades, fluorescent nanoparticles have been thoroughly studied and used in many experiments[109,110]. Conventional single-photon excited fluorescence is based on the excitation of a fluorophore by the short-wavelength visible or ultraviolet light. A major drawback of this photoluminescence is low penetration depth of its short-wavelength excitation light in human tissue[111]. In contrast, low energy near-infrared (NIR) photons with wavelengths ranging from 700 nm to 1000 nm can penetrate biological tissue up to 2 cm, as this spectrum falls within the biological tissue transparency window[112,113]. Moreover, the low energy of NIR photons have minimal adverse effects on normal cells and tissues[112].

However, short-wavelength visible light is preferable for imaging and generation of reactive oxygen species by photosensitisers. Two-photon fluorescent imaging is widely used in microscopy to transform NIR to visible light. Its application scope *in vivo* is limited due to the need for simultaneous absorption of two NIR photons and, consequently, high laser power density (up to 10^9 W/cm^2), which is hard to achieve using standard clinical equipment. Therefore, upconversion photoluminescence, which also can convert NIR radiation to visible light is advantageous, as it uses sequential photons and

requires lower laser power densities (1-10^3 W cm^{-2}) to generate higher-energy visible photons[110,114-116] demanded for imaging and photoactivation of photosensitisers (**Figure 2**).

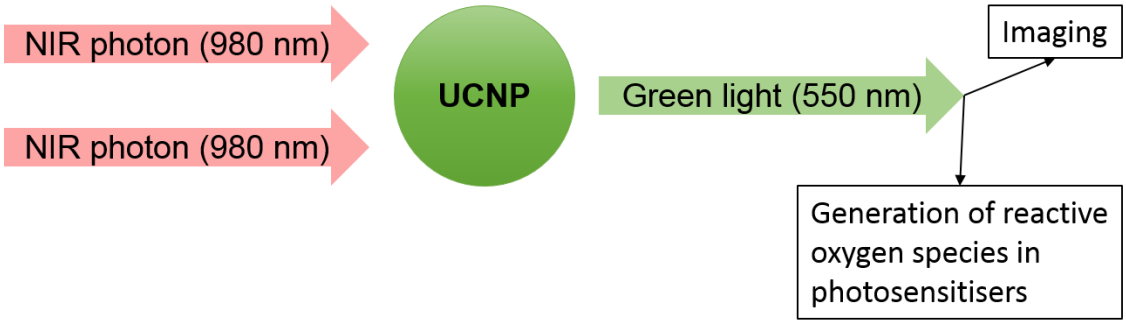

Figure 2. Schematic illustration of the application of upconversion nanoparticles (UCNP) for diagnosis and therapy.

Lanthanide-doped inorganic photoluminescent upconversion nanoparticles, such as $NaYF_4$:Yb,Er, are believed to hold promise for biomedical applications due to their low cytotoxicity and higher photoluminescence efficiency compared to the other photoluminescent agents, such as organic fluorophores and semiconductor quantum dots[117-121]. The key photophysical property of upconversion nanoparticles is energy transfer upconversion (**Figure 3**). Firstly, 980 nm light excites Yb atoms embedded in an inorganic nanocrystal matrix. Yb atom then transfers the absorbed energy to Er atom, which makes a transition to the first excited state. Subsequent second energy transfer from Yb atom excites Er to the next excited state from where Er emits green light with wavelength of approximately 550 nm, when relaxing back to the ground state (**Figure 3**).

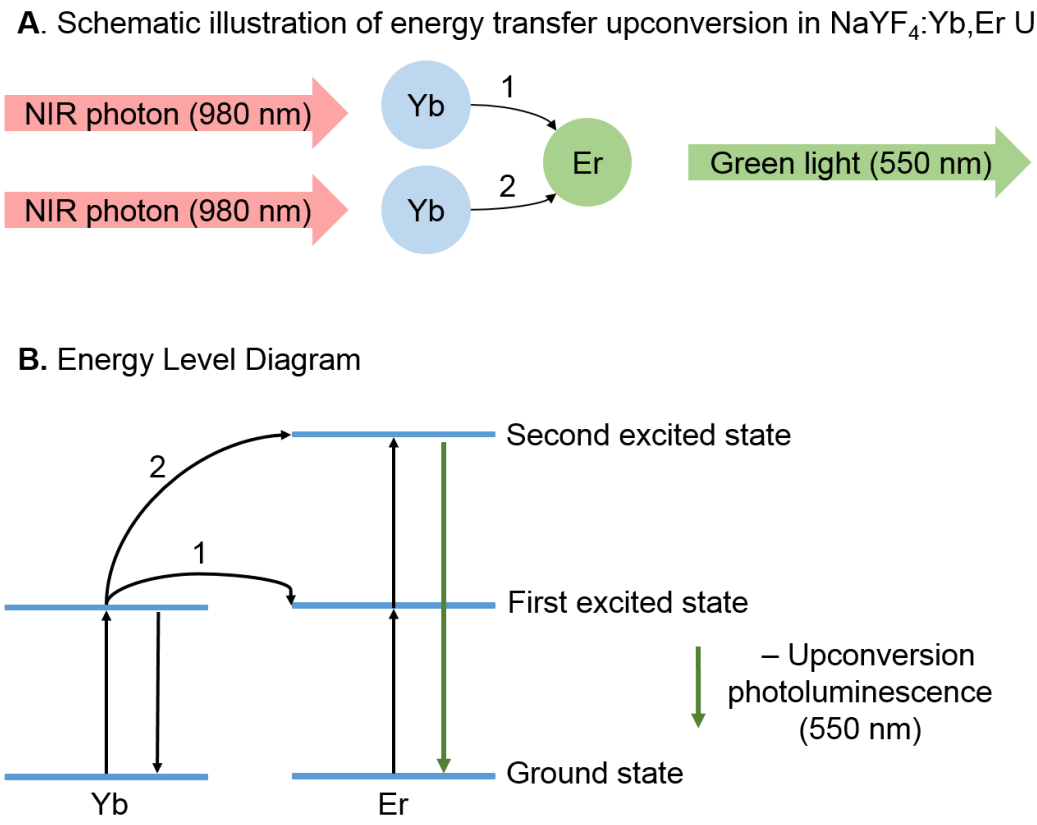

Figure 3. Schematic presentation (**A**) and mechanism (**B**) of energy transfer upconversion in upconversion nanoparticle (UCNP) $NaYF_4$:Yr,Er limited to two-photon upconversion process.

1.3.4.3. Upconversion nanoparticles for theranostics of bladder cancer

Upconversion nanoparticles of the composition $NaYF_4$:Yb:Er are among the most promising platforms for PDD and PDT of bladder cancer. Photophysical properties of these photoluminescent nanoparticles provide high contrast of the labelled structures against the background of strong scattering and autofluorescence of biological tissue[122]. Moreover, upconversion nanoparticles can preferentially accumulate in tumour tissue due to the leaky capillary blood vessels in tumours in virtue of enhanced permeability and

retention effect (EPR)[123]. Coating with silica could allow incorporation of imaging or targeting agents or the most effective individually chosen drugs[116,124-126].

To become a multifunctional photodynamic agent, upconversion nanoparticles need a tumour-targeting unit. Proteins[127], folic acid[128-130] and antibodies[131] were previously used for diagnostic and therapeutic actions of upconversion photoluminescent nanoparticles. Antibodies are preferable as targeting agents, as they will allow adjustment of the affinity of nanoconjugates, depending on the antigen expression of target cells. In combination with monoclonal antibodies, upconversion nanoparticles form targeted upconversion photoluminescent nanoconjugates for imaging and therapeutic applications. Antibody mediated targeting should result in the preferential accumulation of the agent in tumours and avoid side effects caused by the accumulation of a drug in normal tissues. A monoclonal antibody MIL38 supplied by Minomic International Ltd. (Sydney, Australia) had shown high affinity to Glypican-1, which is expressed by urinary bladder cancer cells and has a potential to deliver nanoconjugates to urothelial carcinoma cells.

The choice of a method of the bioconjugation of nanoparticles with antibodies is crucial, as it can affect functioning of antibody. Conventional methods of bioconjugation involving carboxyl activating agents or amine-reactive crosslinking suffer from complexity and poor coordination control of functional biomolecules[132-135].

In this project, we applied a recently developed self-assembling bioconjugation strategy based on a silica-specific solid-binding peptide (linker) that exhibited the high binding affinity towards silica (**Figure 4**)[136]. This linker can be genetically fused to a protein of interest and the resulting recombinant fusion protein (Linker-Protein) binds

strongly to silica-containing materials. Using genetic engineering, the Linker was incorporated into the N-terminus of truncated form of antibody-binding Protein G of Streptococcus strain G148[136]. This bifunctional fusion protein, Linker-Protein G (LPG), has been shown to act as an anchorage point for antibodies at the surfaces of silica-coated nanoparticles[132]. Specific binding to crystallisable fragment (Fc) of an antibody prevents interference with antigen-binding sites (Fab) and happens within minutes, without the need for any chemical modification or physical treatment and allows attachment of desired quantities of antibody for specific applications[132].

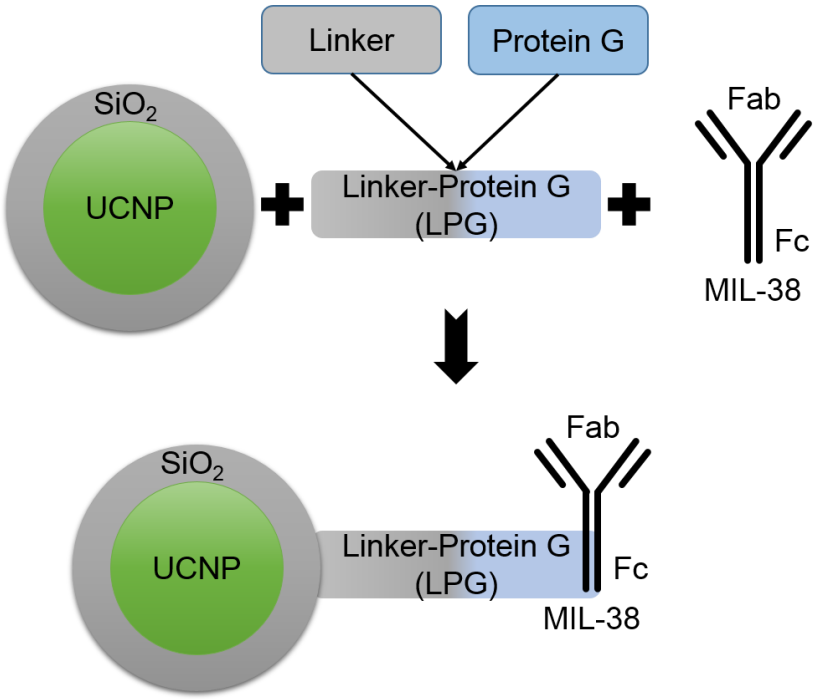

Figure 4. Schematic diagram of bioconjugation of a silica-coated (SiO_2) upconversion nanoparticle (UCNP), Linker-Protein G (LPG) and antibody MIL38 with crystallisable (Fc) and antigen-binding (Fab) fragments. It also shows a targeted upconversion nanoconjugate with oriented binding of MIL38.

1.4. Conclusions of the review of current state of bladder cancer and research objectives of this study

1.4.1. Conclusions of the literature review

The review of existing and emerging techniques in diagnosis and therapy of bladder cancer demonstrated unmet clinical needs of patients with resistant disease. The review also highlighted an incomplete resection, reimplantation of cancer cells and high aggressiveness of a tumour, as potential reasons for recurrence and progression and outlined the ways in which PDD and PDT could improve an outcome of the bladder cancer treatment. Upconversion photoluminescent nanoparticles have a number of unique properties, such as highly efficient conversion of deep-penetrating near-infrared light into visible light and possibility of their conjugation with biomolecules, making them a promising candidate for PDD and PDT. Therefore, these nanoparticles were chosen for this study of targeted labelling of bladder cancer.

It was found that upconversion nanoparticles linked with anti-Glypican-1 monoclonal antibody MIL38 have a potential in targeting urothelial carcinoma cells with the high expression of Glypican-1 (T24). It was also found that one of the most suitable ways of bioconjugation was based on an LPG linker, as it allowed oriented binding of MIL38 to upconversion nanoparticles to produce targeted upconversion nanoconjugates UCNP@SiO_2-LPG-MIL38 for PDD and PDT of bladder cancer (**Figure 5**).

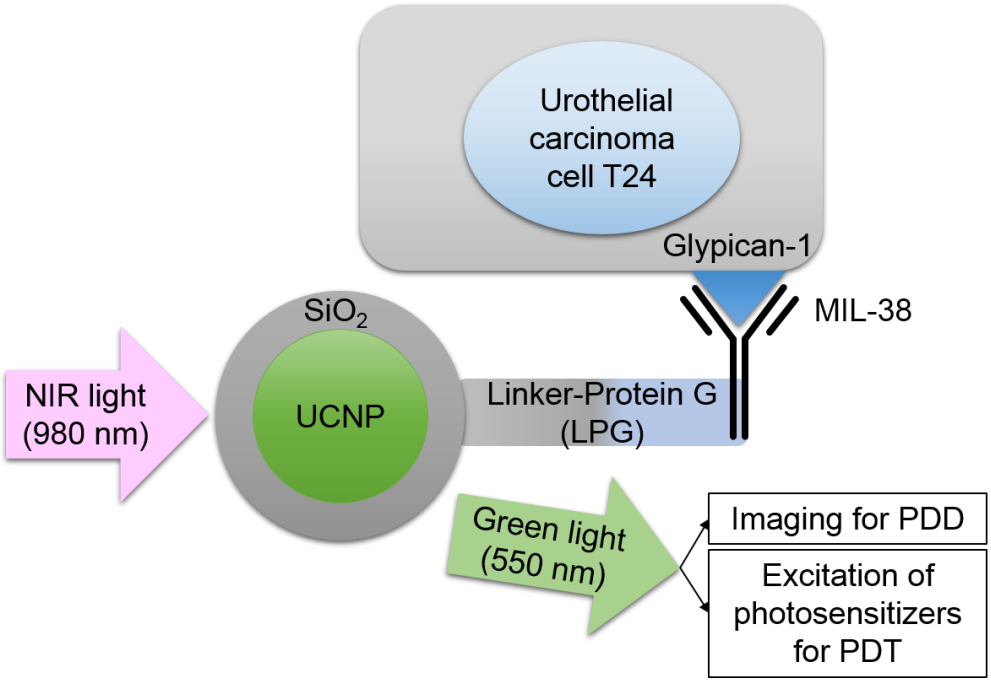

Figure 5. Schematic illustration of the proposed application of targeted upconversion nanoconjugates in PDD and PDT of bladder cancer.

1.4.2. Approach

Upconversion nanoparticles of the composition $NaYF_4$:Yb:Er were chosen as a platform for this research. They were produced and coated with silica to become amenable for further conjugation with biomolecules. To target T24 urothelial carcinoma cells, expressing Glypican-1, silica-coated upconversion nanoparticles (UCNP@SiO_2) were conjugated with a Glypican-1 monoclonal antibody MIL38, by using LPG linker, resulting in targeted upconversion nanoconjugates UCNP@SiO_2-LPG-MIL38.

Specific targeted binding of the targeted nanoconjugates UCNP@SiO_2-LPG-MIL38 was assessed *in vitro* by using T24 human urinary bladder carcinoma cells, which had the high expression of surface proteoglycan Glypican-1. For this purpose, T24 cells and control C3 cells with low expression of Glypican-1 were incubated with these

nanoconjugates. To demonstrate that specificity was caused by a MIL38 antibody, controls included incubation of T24 cells with upconversion nanoparticles conjugated with a control antibody and without an antibody.

To assess the sensitivity and specificity of the targeting, results were analysed by visual quantification of labelled cells in each group. The proportions of labelled cells were then calculated and compared between the groups. To further assess the labelling performance of the targeted upconversion nanoconjugates, we analysed the photoluminescence intensity of single cells after the incubation with nanoconjugates and also carried out group cross-comparison. This analysis was performed by using a confocal laser-scanning microscopy and imaging software.

1.4.3. Research objectives

The main objective of this project was to produce a targeted upconversion photoluminescent nanoconjugate that can specifically bind to Glypican-1 positive urothelial carcinoma cells T24 and render them optically detectable by means of photoluminescence. In order to achieve this objective, we needed to:

1. Produce upconversion nanoparticles of the composition $NaYF_4$:Yb:Er relying on their low cytotoxicity and strong upconversion photoluminescence;
2. Coat these nanoparticles with a layer of silica to make them amenable for further conjugation with biomolecules;
3. Conjugate these nanoparticles with a Glypican-1 monoclonal antibody MIL38 without affecting upconversion photoluminescence of the nanoparticle and affinity to the antibody;

4. Establish growth conditions of Glypican-1 high and Glypican-1 low urothelial carcinoma cell lines T24 and C3;
5. Investigate the binding of targeted upconversion nanoconjugates UCNP@SiO_2-LPG-MIL38 to Glypican-1 high (T24) and Glypican-1 low (C3) urothelial carcinoma cells to assess their specificity;
6. Investigate the binding of control upconversion nanoconjugates without an antibody or conjugated with a different antibody to T24 urothelial carcinoma cells, in order to assess the role of a monoclonal antibody MIL38 in targeting urothelial carcinoma.

Chapter 2: Production and characterisation of targeted upconversion photoluminescent nanoconjugates

2.1. Introduction

To address the first two objectives of this project, we had to produce and characterise targeted upconversion photoluminescent nanoconjugates. The review of the literature concluded that photoluminescent nanomaterials and especially upconversion nanoparticles have a great potential in diagnosis and therapy of bladder cancer.

Therefore, we synthesised lanthanide-doped upconversion nanoparticles of composition $NaYF_4$:Yb,Er, functionalised them with LPG linker, to prepare for a conjugation with an antibody, and conjugated them with anti-Glypican-1 monoclonal antibody MIL38 to target Glypican-1 positive urothelial carcinoma cells.

The protocol of LPG-mediated conjugation of upconversion nanoparticles with an antibody was developed and applied previously[136,137]. However, modification of upconversion nanoparticles and antibody in this project were different from the method described previously. Also, to the best of our knowledge, this is the first ever investigation of the bioconjugation of anti-Glypican-1 monoclonal antibody MIL38 with an upconversion nanoparticle.

This chapter describes the production of upconversion photoluminescent nanoparticles and their conjugation with a monoclonal antibody MIL38.

2.2. Materials and methodologies applied in the production, characterisation and conjugation of upconversion nanoparticles

2.2.1. Reagents for production of upconversion nanoconjugates

Upconversion nanoparticles were prepared by using Yttrium(III) chloride hexahydrate ($YCl_3 \cdot 6H_2O$; 99.999%), ytterbium(III) chloride hexahydrate ($YbCl_3 \cdot 6H_2O$; 99.9%), erbium(III) chloride hexahydrate ($ErCl_3 \cdot 6H_2O$; 99.9%), sodium hydroxide (NaOH; ≥97.0%), ammonium fluoride (NH_4F; ≥98.0%), oleic acid (OA; 90%), 1-octadecene (ODE; 90%), cyclohexane (99.5%), tetraethylorthosilicate (TEOS), Igepal CO-520, ammonium hydroxide solution (NH_4OH; 30%). All these reagents were supplied by Sigma-Aldrich Chemicals (Sydney, Australia) and did not require further purification.

Tris(hydroxymethyl)aminomethane (Sigma-Aldrich Chemicals) and UltraPure Distilled Water (Invitrogen) were applied in the preparation of Tris-buffered saline required for conjugation of upconversion nanoparticles with LPG and MIL38.

Cryptosporidium monoclonal antibody CRY104 and LPG linker were kindly provided by A. Sunna and A. Care (Department of Chemistry and Biomolecular science and ARC Centre of Excellence for Nanoscale BioPhotonics, Macquarie University). Glypican-1 monoclonal antibody MIL38 was produced and kindly provided by Minomic International Ltd. (Sydney, Australia).

2.2.2. Equipment used in characterisation of upconversion nanoparticles

Transmission electron microscopy of upconversion nanoparticles was performed using a Philips CM10 electron microscope. This microscope had a resolution of 0.2 nm, which allowed the high-quality visualisation of their shape and of the silica layer on their surface. Size distribution of upconversion nanoparticles on transmission electron microscopy images was analysed by using the ImageJ software. Hydrodynamic diameter by dynamic light scattering and zeta potential were measured on a Zetasizer Nano ZS90 (Malvern instruments Ltd.). The intensity of the photoluminescence of upconversion nanoparticles was measured using a spectrofluorometer Fluorolog-Tau3 (Jobin Yvon-Horiba) equipped with an external 978-nm fibre-coupled diode laser. Microcentrifuge 5415R (Eppendorf) and 120 W 40 kHz and ultrasonic cleaner PS20 (Jeken Ultrasonic Cleaner Ltd.) were used for washing of upconversion nanoparticles and their functionalisation with LPG and antibodies. Solutions containing required concentrations of the nanoparticles were prepared by using a balance UMX2 Ultra-microbalance (Mettler Toledo). The pH level of Tris-buffered saline was adjusted by using pH meter pHTestr 10 (Thermo Scientific).

2.2.3. Methodology of synthesis of upconversion nanoparticles

Upconversion nanoparticles of the composition $NaYF_4$, doped with 18% Yb and 2% Er ($NaYF_4$:Yb,Er), were synthesised as per previously published protocol[116]. YCl_3 (0.8 mmol), $YbCl_3$ (0.18mmol) and $ErCl_3$ (0.02mmol) were added to a flask containing 6 mL of OA and 15 mL of Octadecene, heated to 160 °C for 30 min to dissolve the lanthanide salts under an argon flow. After the heating, the mixture was cooled to room temperature. NaOH (2.5 mmol) and NH_4F (4 mmol) dissolved in 10 mL of methanol were

then added to the flask and stirred for 30 min at room temperature. Subsequently, this mixture was heated to 110 °C for 30 min to remove the residual methanol and water. For the following 1 hour, this mixture was heated to 310 °C under argon flow with stirring and cooled to room temperature afterwards. Finally, before being coated with silica, nanoparticles were washed three times with ethanol/methanol (1:1, v/v) solution and suspended in cyclohexane to obtain the particle suspension.

Upconversion nanoparticles were then coated with a layer of silica. Firstly, coating with silica converts the hydrophobic nanoparticles into hydrophilic. Secondly, the silica coating improves the colloidal stability of the nanoparticles, increasing solubility and decreasing their aggregation in water and in physiological buffers. Thirdly, the silica layer allows efficient functionalisation of these nanoparticles with other molecules, such as photosensitisers for photodynamic therapy, antibodies for targeted action and immunomodulation or various drugs to use upconversion nanoparticles as nanocarries[124,125,138-142].

Silica coating was performed as following: 5 mL of $NaYF_4$:Yb,Er (0.1 mmol) cyclohexane suspension and 5 mL of Igepal CO-520 (0.5 mL) cyclohexane solution were mixed in a one-neck flask and kept sealed and stirring at room temperature for 3 h. After that, 500 μL of ammonium hydroxide solution was added to the mixture and kept stirring for another 2 h. The following step was the slow injection of 40 μL of Tetraethyl orthosilicate (2 μl/min) to the reaction mixture. The stirring was continued for 24 h before the addition of ethanol to precipitate the nanoparticles. The obtained silica-coated upconversion nanoparticles (UCNP@SiO_2) were then washed three times with 100 % ethanol and another three times with ultrapure distilled water. In each washing an Eppendorf tube with nanoparticles was centrifuged for 7 min at the speed of 13100 × g,

supernatant was replaced with 1 mL of ethanol or water and nanoparticles were sonicated for 10 min in an ultrasonic water bath.

A transmission electron microscope (Philips CM10) was used to visualise distribution of upconversion nanoparticles with and without silica coating. The hydrodynamic diameter of upconversion nanoparticles was measured by using dynamic light scattering via a Zetasizer Nano ZS90 (Malvern instruments Ltd.), which was also used to measure zeta potential of the particles. Zeta potential is the potential difference between electric double layer of dispersed nanoparticles and the layer of dispersant around them. This electric double layer consists of ions with different charge and correlates with surface potential of the particle, electrostatic repulsive forces between particles and, therefore, their colloidal stability[143].

2.2.4. Conjugation of upconversion nanoparticles with LPG linkers

In order to conjugate upconversion nanoparticles with antibodies, nanoparticles firstly had to be functionalised with LPG linker, which was kindly provided by Andrew Care and Anwar Sunna. This linker is a bifunctional fusion protein that consists of a solid-binding peptide linker and Protein G from Streptococcus strain G148[132,136,144]. The affinity of the solid-binding peptides towards solid surfaces is caused by a combination of hydrophobic, electrostatic, polar and other multiple non-covalent interactions[132,136]. The solid-binding peptide linker employed in this project has demonstrated strong binding affinity towards surface materials containing silica, such as silica nanoparticles or nanoparticles coated with a silica layer[132,136,137,144]. The negative charge of the silica surfaces and positive charge of the linker made by a number of basic lysine and arginine residues underpins this binding[145]. Moreover, an intrinsic structural disorder of this linker

increases its flexibility and plasticity. As a result, it further promotes electrostatic interactions between positively charged residues of the peptide and negatively charged silica-containing nanomaterials[136,144].

Protein G, purified from Streptococcus strain G148, is an antibody-binding protein that has a strong avidity towards a variety of immunoglobulins[144,146,147]. This protein binds to the crystallisable fragment (Fc) of Ig-G antibody and leaves the antigen-binding fragment (Fab) available for recognition and binding to antigen. Protein G was genetically fused with a solid-binding peptide linker, resulting in a linker-protein G (LPG) with a region binding to silica-containing materials, such as silica-coated upconversion nanoparticles, and a region that allows oriented immobilisation of Ig-G antibodies, such as anti-Glypican-1 monoclonal Ig-G antibody MIL38.

Before conjugation with LPG, silica-coated upconversion nanoparticles were washed three times with 100% ethanol and another three times with ultrapure distilled water. Nanoparticles were centrifuged in an Eppendorf tube for 7 min at 13,100 × g; supernatant was removed and replaced by 1 mL of ultrapure water or ethanol, respectively; nanoparticles were then sonicated in an ultrasonic cleaner water bath for 10 minutes.

Conjugation of nanoparticles with LPG required the use of 100mM Tris-buffered saline (pH=7.5). To prepare this buffer, 7.88 g of Tris(hydroxymethyl)aminomethane (Sigma-Aldrich Chemicals) was added to 400 mL of distilled water. Then, under a control of a pH meter pHTestr 10 (Thermo Scientific), pH of the solution was adjusted from 5 to 7.5, by adding in 0.1 M sodium hydroxide solution.

Linking of LPG to upconversion nanoparticles consisted of a number of simple mixing and washing steps. Firstly, 1 mL ethanol solution containing 1 mg of nanoconjugates was produced by using the UMX2 Ultra-microbalance (Mettler Toledo). Then, nanoparticles were washed three times with 100 mM Tris-HCl buffer (pH=7.5), and resuspended in 400 µl of Tris-HCl buffer containing 20 µg of LPG. After that, this mixture was rotated at 4°C for 30 min and centrifuged at 7000 × g to collect the LPG bound nanoconjugates (UCNP@SiO_2-LPG) and to separate the unbound LPG. Before functionalisation with an antibody, nanoconjugates UCNP@SiO_2-LPG were washed two more times with Tris-buffered saline via centrifugation and sonication. In order to prevent overheating of LPG, all procedures were performed at low temperatures. Water bath sonicator was filled with ice to maintain the low temperature, and the centrifugation and incubation were performed at 4 ºC

Successful conjugation of upconversion nanoparticles with a positively charged LPG was confirmed by a positive shift of zeta potential, which was measured using a Zetasizer Nano ZS90 (Malvern instruments Ltd). Measurement of zeta potential was performed by using 0.8 mL of 100 µg/mL solution of nanoconjugates UCNP@SiO_2-LPG in Tris buffer.

2.2.5. Production of the targeted upconversion nanoconjugates

MIL38 is a monoclonal antibody, that was initially raised against urothelial carcinoma cells and was previously known as BLCA-38[148,149]. The target of this antibody was recently discovered to be a proteoglycan Glypican-1[150,151]. Glypican-1 is a cell membrane heparan sulfate proteoglycan. This proteoglycan consists of a variable number of heparan sulphate chains and a core protein attached to a phospholipid bilayer via a

glycosylphosphatidylinositol linker[150,152,153]. Glypican-1 is a growth factor receptor and, therefore, participates in the control of growth and division of cells[152]. In addition to urothelial carcinoma, the presence of this proteoglycan was previously reported in prostate[150,151,154-156], pancreatic[157-160], oesophageal[161], breast[162] and brain[163,164] cancers. In this project, the specificity of anti-Glypican-1 antibody MIL38 towards urothelial carcinoma cells was utilised for their targeted labelling by upconversion nanoparticles coupled to MIL38 and termed targeted upconversion nanoconjugates.

After washing, LPG-bound nanoconjugates UCNP@SiO_2-LPG were ready for functionalisation by a monoclonal antibody MIL38. These nanoconjugates were resuspended by sonication and incubated with antibody MIL38 with ratio of 20 μg of the antibody per 1000 μg of nanoparticles with rotation for 30 min at 4°C. Finally, targeted nanoconjugates UCNP@SiO_2-LPG-MIL38 were separated from unbound antibodies by centrifugation and two washings with Tris buffer. Resulting nanoconjugates were redispersed in 1040 μL of Tris-buffered saline (pH=7.5) to produce the 1 mg/mL suspension of targeted upconversion nanoconjugates UCNP@SiO_2-LPG-MIL38.

Characterisation of UCNP@SiO_2-LPG-MIL38 included the measurement of zeta potential and hydrodynamic diameter using Zetasizer and photoluminescence spectrum using a spectrofluorometer Fluorolog-Tau3 (Jobin Yvon-Horiba) equipped with an external 978-nm laser.

2.3. Results of the synthesis and conjugation of upconversion nanoparticles

2.3.1. Upconversion nanoparticles amenable for conjugation with biomolecules

A solvothermal decomposition method was used to synthesise upconversion nanoparticles $NaYF_4$:Yb,Er (as described in section 2.2.3)[137]. Nanoparticles had spherical shape, were monodispersed (**Figure 6, A**) and had a mean size of 33.1 nm with a narrow size distribution (standard deviation = 1.5 nm) (**Figure 6, C**). Then these nanoparticles were coated with a layer of silica using water-in-oil microemulsion method (as described in section 2.2.3)[165].

Transmission electron microscopy demonstrated the successful coating with silica, resulting in improved dispersion of upconversion nanoparticles (**Figure 6, B**). An increase of their average diameter (measured by imaging software) from 33.1 ± 1.5 nm to 41.2 ± 2.4 nm (**Figure 6, D**) demonstrated that the thickness of the silica layer was approximately 4 nm. The shape of the nanoparticles after silica coating remained spherical (**Figure 6, A and B**).

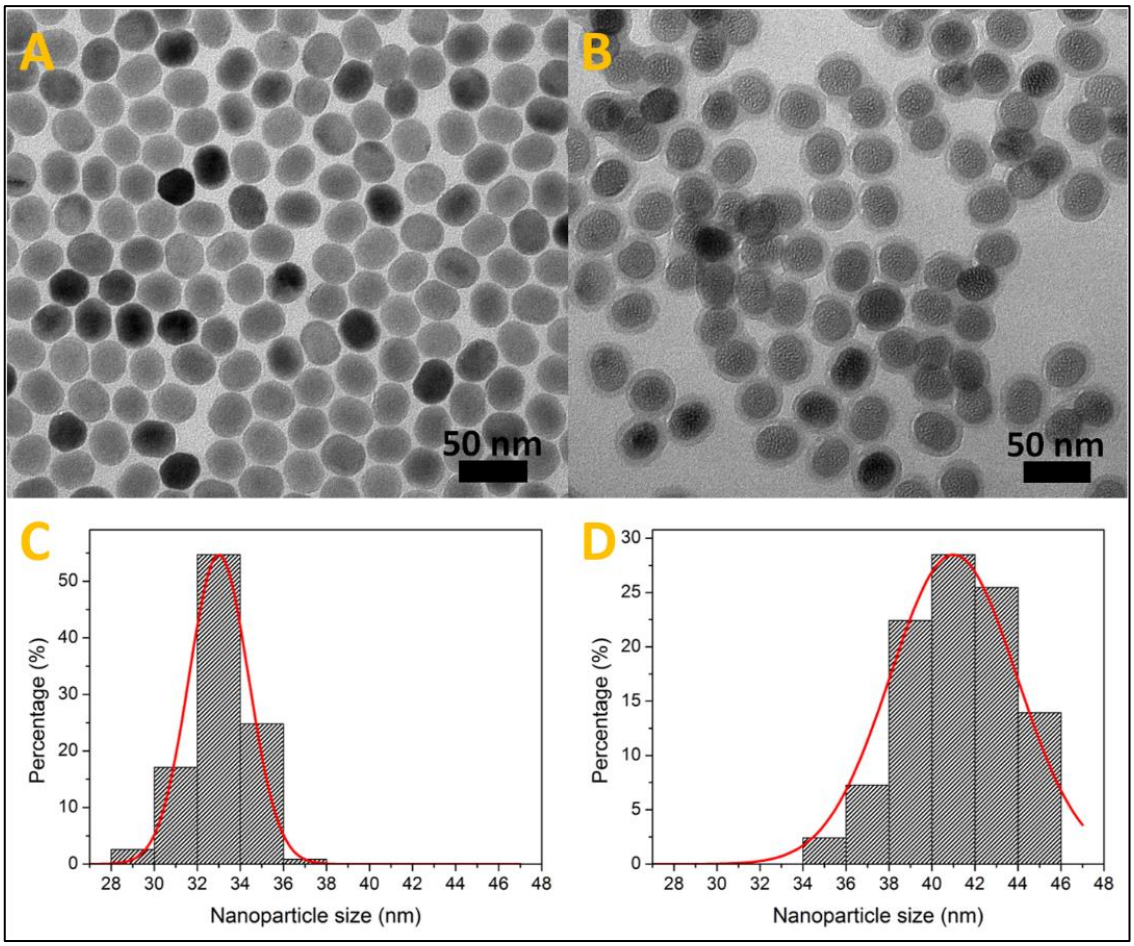

Figure 6. Transmission electron microscopy of upconversion nanoparticles $NaYF_4$:Yb,Er before **(A)** and after **(B)** the coating with a silica layer. **(C)** and **(D)** show the size distribution of nanoparticles before and after the silica coating.

Characterisation of the silica-coated upconversion nanoparticles also included the measurement of their zeta-potential and hydrodynamic diameter by dynamic light scattering using a Zetasizer system (Malvern instruments Ltd.). Resulting nanoparticles displaced a negative zeta-potential of -16.6 mV and mean hydrodynamic diameter (measured by the dynamic light scattering) of 227 nm, which was probably affected by a limited number of large clusters, whereas the vast majority of nanoparticles had a hydrodynamic diameter around 100 nm (**Figure 7**).

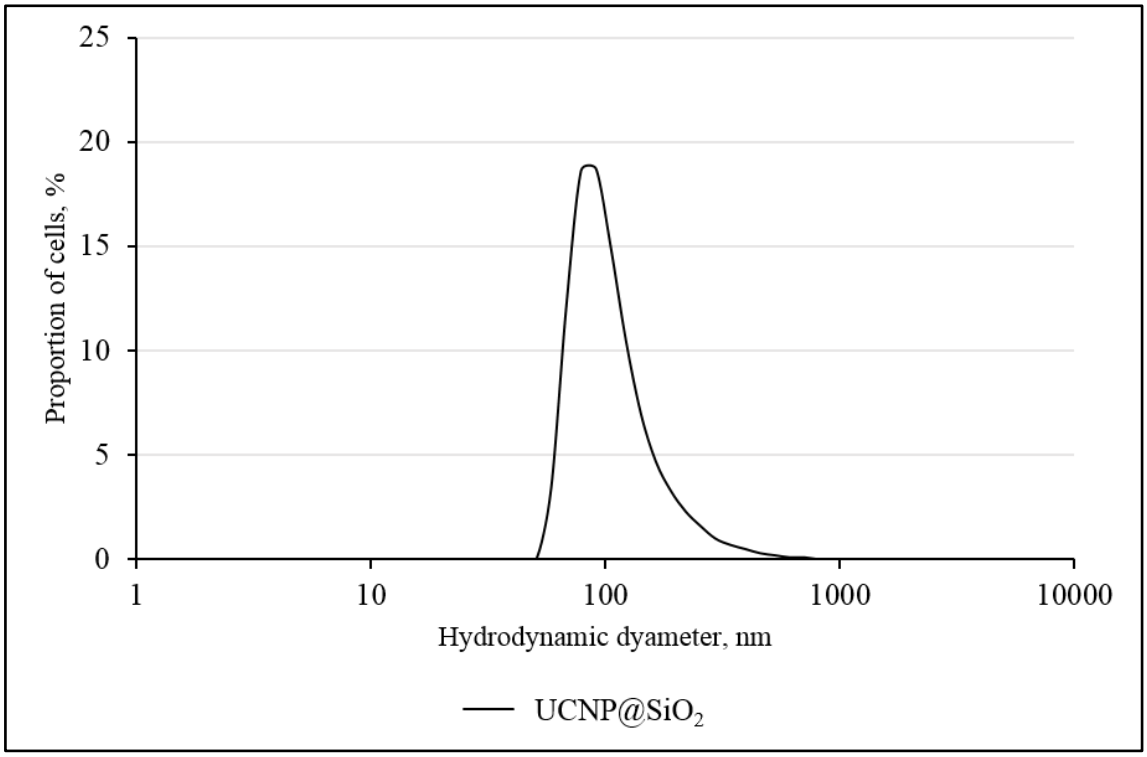

Figure 7. Size distribution of silica-coated upconversion nanoparticles (UCNP@SiO_2) measured by the dynamic light scattering.

One of the most advantageous properties of the silica-coated nanoparticles is upconversion photoluminescence. These nanoparticles emit bright green light under the illumination with a 980-nm near-infrared laser. The upconversion photoluminescence of as-synthesised silica-coated nanoparticles measured by a spectrofluorometer Fluorolog-Tau3 (Jobin Yvon-Horiba) equipped with a 978-nm laser featured two bands in green (535-555 nm) and red (645-679 nm) regions of the emission spectrum, with the green band being almost two-fold brighter than that of the red band, as shown in **Figure 8**. Peaks of green light at 550 nm and red light at 650 nm are characteristic to Yb/Er co-doped upconversion nanoparticles[137].

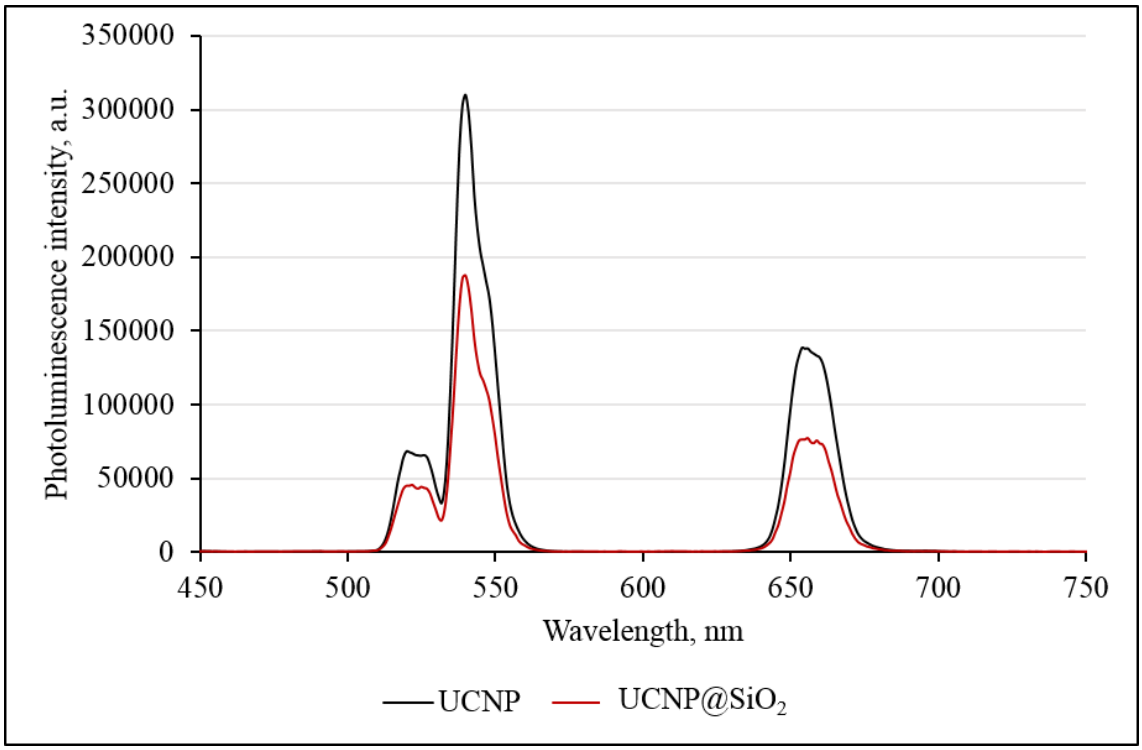

Figure 8. Photoluminescence spectra of upconversion nanoparticles under the excitation with a near-infrared 980-nm laser before (UCNP) and after coating with silica (UCNP@SiO_2).

As one can infer by comparing two curves in **Figure 8**, the coating of upconversion nanoparticles with a silica (SiO_2) layer slightly affected their photoluminescence properties, while retaining characteristic spectral features. Nonetheless, the optical properties of UCNPs were largely preserved after silica coating, and particles displayed satisfactory brightness for the subsequent observation of cellular labelling. Slight decrease of their photoluminescence intensity caused by the coating with a silica layer is consistent with literature and may be caused by absorption of light by silica and by its quenching properties[166].

2.3.2. Upconversion nanoparticles conjugated with LPG

In order to conjugate silica-coated upconversion nanoparticles with an antibody, they were, firstly, functionalised by the LPG linker. LPG was attached to the nanoparticles following a previously developed protocol[136,137]. Functionalisation by a positively charged LPG was confirmed by a reduction of the negative zeta potential charge of the nanoparticles from -16.6 mV to -9.65 mV (**Table 1**). Resulting upconversion nanoparticles conjugated with LPG (UCNP@SiO_2-LPG) were washed from unbound LPG and were ready for bioconjugation with similar amounts of anti-Glypican-1 Ig-G antibody MIL38 and control cryptosporidium Ig-G antibody CRY104.

Table 1. Zeta-potentials of silica-coated upconversion nanoparticles (UCNP@SiO_2), LPG bound nanoconjugates (UCNP@SiO_2-LPG) and targeted upconversion nanoconjugates (UCNP@SiO_2-LPG-MIL38)

Nanoparticle/nanoconjugate	Zeta potential, mV
UCNP@SiO_2	-16.6
UCNP@SiO_2-LPG	-9.65
UCNP@SiO_2-LPG-MIL38	-5.75

2.3.3. Targeted photoluminescent upconversion nanoconjugates

The anchoring of LPG on the surface of upconversion nanoparticles allowed their simple bioconjugation with monoclonal antibodies MIL38. The success of the conjugation was confirmed by a positive shift of the zeta potential of UCNP@SiO_2-LPG (**Table 1**) and an increase of the hydrodynamic diameter of nanoconjugates (**Figure 9**).

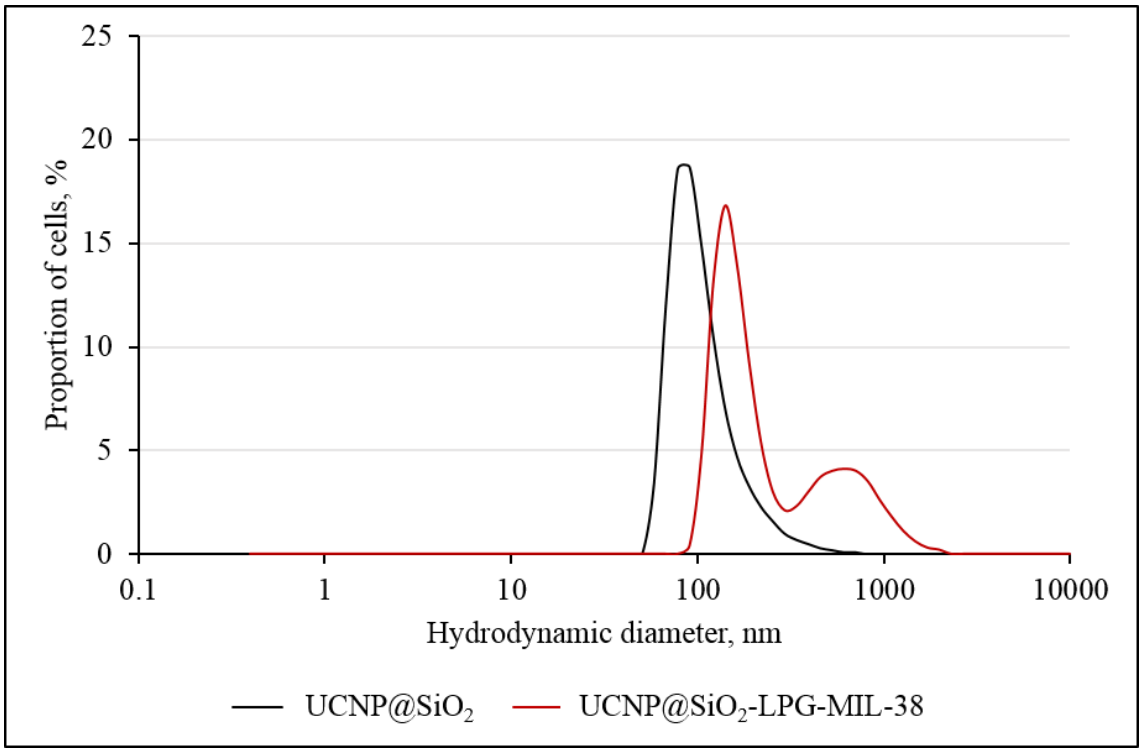

Figure 9. Size distribution of silica-coated upconversion nanoparticles (UCNP@SiO_2) and targeted nanoconjugates UCNP@SiO_2-LPG-MIL38 measured by the dynamic light scattering.

The decrease of the surface charge, following the binding of LPG, was noted, which can be explained by the highly positive charge of LPG in neutral pH (isoelectric point of LPG, 11.2), which compensated the negative charge of the silica-coated upconversion nanoparticles. The binding of MIL38 further decreased the absolute value of the surface charge, which can be explained by the thickening of Stern layer due to the antibody attachment.

The increase of the mean hydrodynamic diameter of the antibody-coupled targeted upconversion nanoconjugates UCNP@SiO_2-LPG-MIL38 can be interpreted by the attachment of MIL38 to the surface of nanoparticles and by some degree of aggregation (as can be seen by a secondary peak centred at ~700 nm - see **Figure 9**). This

aggregation was likely attributed to the slight decrease of the overall surface charge, which provided insufficient electrostatic repulsion to prevent the close-range nanoparticle interaction.

Upconversion photoluminescence intensity decreased slightly after the bioconjugation with antibody (**Figure 10**). However, the emission spectrum remained unchanged, with targeted upconversion nanoconjugates UCNP@SiO_2-LPG-MIL38 featuring the characteristic green and red photoluminescence bands under the 980-nm excitation.

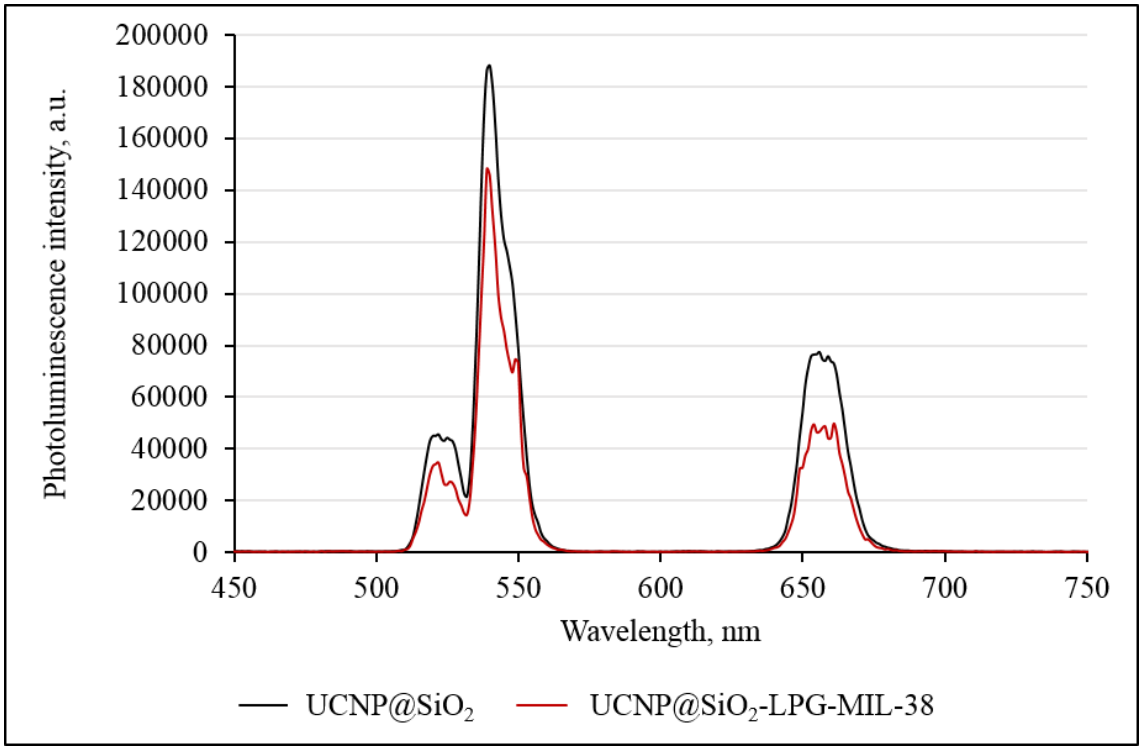

Figure 10. Emission spectra of silica-coated upconversion nanoparticles (UCNP@SiO_2) and targeted upconversion nanoconjugates (UCNP@SiO_2-LPG-MIL38) under excitation by an 980-nm laser.

Overall, targeted nanoconjugates UCNP@SiO_2-LPG-MIL38 were produced and upconversion photoluminescence was not affected considerably. In order to investigate targeting ability of these nanoconjugates, they were further incubated with urothelial carcinoma cells.

2.4. Conclusions

In summary, a method of the production of targeted upconversion nanoconjugates, which was described here, had three steps. The first step was production of upconversion nanoparticles $NaYF_4$:Yb,Er and their coating with a silica layer. Characterisation of nanoparticles demonstrated effectiveness of the method and their suitability for further conjugation. Following steps were the attachment of LPG linkers to silica-coated upconversion nanoparticles and the conjugation of LPG-bound nanoconjugates UCNP@SiO_2-LPG with a monoclonal antibody MIL38, which were also highly effective and affected the upconversion photoluminescence insignificantly. The success of the conjugation was confirmed at each step by alteration of the zeta potential, hydrodynamic diameter and photoluminescence spectrum. As a result, we produced targeted upconversion photoluminescent nanoconjugates suitable for investigation of the targeted labelling of urothelial carcinoma cells T24 and C3.

Chapter 3: Culturing and characterisation of urothelial carcinoma cell lines T24 and C3

3.1. Introduction

The previous chapter concisely described the production and characterisation of targeted upconversion nanoconjugates UCNP@SiO_2-LPG-MIL38 with proposed affinity towards Glypican-1 positive urothelial carcinoma cells. To investigate the sensitivity and specificity of the binding of these nanoconjugates to cells expressing Glypican-1, we incubated them with urothelial carcinoma cell line, with high expression of Glypican-1 (T24) and urothelial carcinoma cell line with low expression of Glypican-1 (C3). This chapter describes the origin of these cell lines, their main characteristics and optimisation of their culturing conditions for this experiment.

3.2. Materials and methods applied in the culturing of T24 and C3 urothelial carcinoma cell lines

3.2.1. Reagents used for cell culturing

Following products were used in cell culturing: Fetal Bovine Serum (Sigma-Aldrich Chemicals); sterile-filtered trypsin-EDTA solution 0.25%, containing 2.5 g porcine trypsin and 0.2 g EDTA • 4Na per litre of Hanks′ Balanced Salt Solution with phenol red (Sigma-Aldrich Chemicals); RPMI-1640 medium with sodium bicarbonate, without L-glutamine (Sigma-Aldrich Chemicals); and Phosphate-buffered saline (PBS) pH7.2 (Gibco). For, the investigation of the influence of coverslip coating on adhesion and growth of urothelial carcinoma cells T24 and C3, coverslips were coated by Poly-D-

lysine hydrobromide (Sigma). Cells were fixed by methanol-free 16% Formaldehyde (Thermo Scientific). After the incubation of cells with nanoconjugates, coverslips were mounted of slides using ProLong Diamond Antifade Mountant with DAPI (Thermo Scientific).

3.2.2. Equipment used for cell culturing and investigation

T24 and C3 cells were cultured in a CO_2 Incubator Heracell 150i (Thermo Scientific) and aseptically handled in a Biological Safety Cabinet Herasafe KS (Thermo Scientific). Rectangular Canted Neck Cell Culture Flask with Vented Cap (Falcon) and a benchtop centrifuge Allegra X-15R (Beckman Coulter) were also used for cell culturing. Counting of the cells was performed by using an automated cell counter Countess C10281 (Invitrogen). Imaging of live T24 and C3 cells was performed by an inverted microscope ECLIPSE TS100 (Nikon) equipped with a microscope camera controller Digital Sight DS-L3 (Nikon), allowing fast transfer of images to a desktop computer (**Figure 11**).

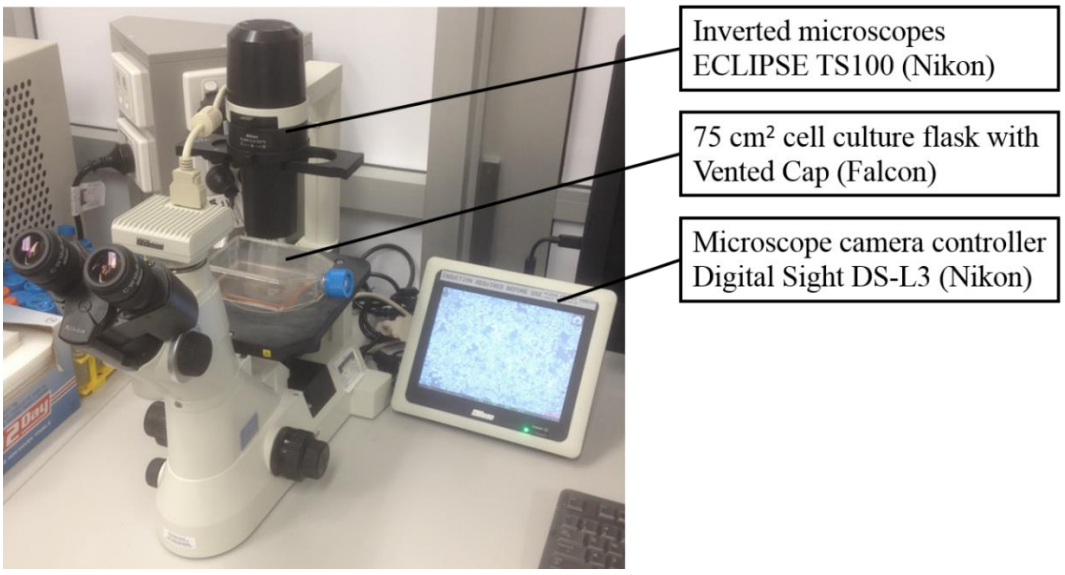

Figure 11. Imaging of live T24 cells on inverted microscopes ECLIPSE TS100 (Nikon) equipped with a microscope camera controller Digital Sight DS-L3 (Nikon)

3.2.3. Origin of T24 and C3 urothelial carcinoma cell lines

T24 and C3 urothelial carcinoma cell lines were kindly provided by Minomic International Ltd. These cell lines were chosen for this experiment due to the high expression of surface proteoglycan Glypican-1 on the membrane of T24 cells[167] and low expression of Glypican-1 by C3 cells[150].

T24 urothelial carcinoma cell line was derived in 1970 by Bubenik *et al*. from 82-year-old female patient with a muscle-invasive (T3), grade III urothelial carcinoma of the urinary bladder[168]. Initially, her bladder cancer was diagnosed in 1962 and she was then unsuccessfully treated by multiple transurethral resections and fulgurations. In 1970, the tumour reached grade III and invaded muscle layer. This tumour was then resected and sample was taken for a cell culture collection. The patient died seven months later from myocardial infarction, with no clinical signs of urothelial carcinoma metastasises[168].

Urothelial carcinoma cell line C3 is a cloned subline of cell line UCRU BL 17Cl[96]. UCRU BL 17Cl cell line was sourced from a 69-year-old male patient with an invasive, stage T4b, grade III urothelial carcinoma[97]. This tumour was resistant to cisplatin and radiotherapy and resulted in a death of the patient four months later. Initially, establishment of a cell line from the tumour was unsuccessful. After that, cells from a biopsy were implanted into a nude mouse and a cell line UCRU BL 17Cl was then established from this xenograft.

3.2.4. *In vitro* culturing of T24 and C3 urothelial carcinoma cell lines

Frozen cells were thawed for two minutes in a water bath at 37 ºC and seeded into a 25 cm^2 and then a 75 cm^2 rectangular cell culture flasks with vented cap (Falcon). The

choice of media for the cell lines was based on a recommendation from Minomic International Ltd. T24 and C3 cells were cultured in a Roswell Park Memorial Institute (RPMI) 1640 Medium supplemented with 10% and 20% of FBS, respectively. Both cell lines were split twice a week, as was also recommended by Minomic International Ltd. Daily monitoring and live-cell imaging of T24 and C3 cells by an inverted microscope ECLIPSE TS100 (Nikon) equipped with a microscope camera controller allowed analysis of their morphology and growth patterns.

3.3. Results of the investigation and optimisation of the culturing of T24 and C3 urothelial carcinoma cells

3.3.1. Characteristics of T24 and C3 urothelial carcinoma cell lines

3.3.1.1. Immunological characterisation of T24 and C3 cells

In order to demonstrate the ability of upconversion nanoconjugates coupled to MIL38 antibodies to target Glypican-1 positive urothelial carcinoma, we used Glypican-1 high T24 and Glypican-1 low C3 (control) urothelial carcinoma cell lines kindly provided by Minomic International Ltd. Affinity a monoclonal antibody MIL38 towards urothelial carcinoma cells T24 was described previously[167] and was confirmed by the results of the flow cytometry analysis provided by Minomic International Ltd.

Flow cytometry was used to assess affinity of MIL38 towards T24 and C3 cells. Firstly, T24 and C3 cells were incubated with antibodies MIL38 and washed twice to remove unbound antibodies. Then, they were incubated with secondary antibodies, which were conjugated to a fluorescent label. These fluorescent secondary antibodies bound to MIL38 antibodies attached on the surface of cells. As a result, cells with MIL38 on their

surface were fluorescently labelled. T24 and C3 cells were subsequently analysed using a flow cytometer to assess their fluorescence intensity as a sign of the binding of MIL38 to their surface. At least ten thousand cells were analysed in each group. Results of this analysis are presented in **Figure 12**, which shows the distribution of the fluorescence intensity of T24 and C3 cells.

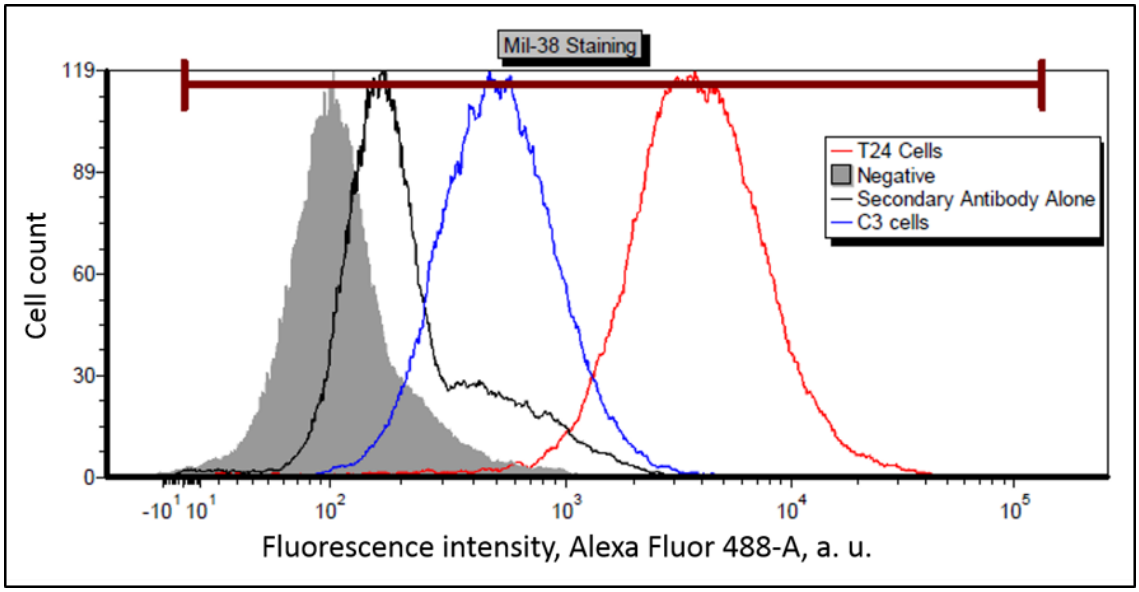

Figure 12. Flow cytometry analysis performed by Minomic International Ltd., demonstrated the binding of MIL38 antibody to T24 cells and minimal binding to C3 cells. Secondary antibody alone was used as a control.

Flow cytometry analysis performed by Minomic International Ltd. demonstrated that T24 cells (**Figure 12**, red histogram) had stronger fluorescence than that of C3 cells with a median fluorescence intensity of 3531.74 a.u. versus 482.16 a.u. Minimal binding to C3 cells was also observed (**Figure 12**, blue histogram). Secondary antibody alone was used as the control for this analysis (**Figure 12**, black histogram).

Morphology of T24 and C3 cells

For further investigation of the targeted labelling, urothelial carcinoma cells T24 were going to be incubated with targeted nanoconjugates UCNP@SiO_2-LPG-MIL38. To assess the specificity of their binding, the same nanoconjugates had to be incubated with C3 cell line. Daily monitoring and live-cell imaging of T24 and C3 cells by an inverted microscope ECLIPSE TS100 (Nikon) equipped with a microscope camera controller allowed analysis of their morphology and growth patterns to optimise culturing conditions for the following experiment (**Figure 11**).

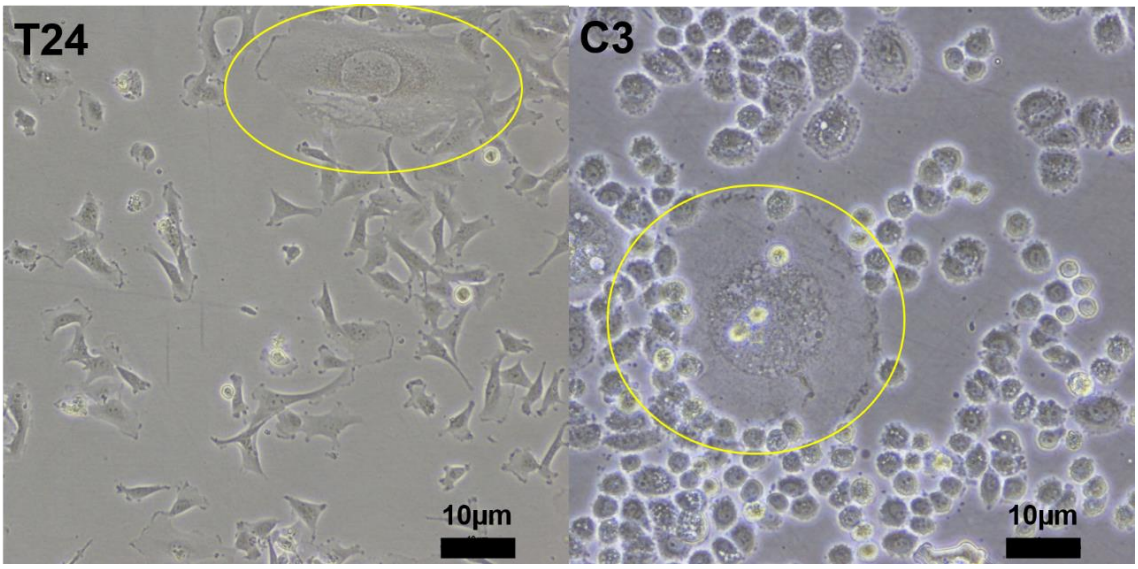

Figure 13. Abnormal cells observed via microscopy of T24 (left) and C3 (right) cell lines growing in 75-cm^2 flasks.

T24 and C3 cells featured different shape. T24 cells were polygonal or spindle-shaped, spreading wider in the culturing flask, while C3 cells looked smaller and more rounded (**Figure 13**). Interestingly, abnormally large spherical cells occasionally containing two or more nuclei were noted in both cell lines. In T24 cell line, these abnormal cells were

observed in the regions with the lower cell density, while in C3 cell culture, such cells were evenly spread.

As a result, the cell culturing was optimised before carrying out labelling experiments, so that the growth was relatively stable and the number of abnormal cells minimal.

3.3.2. Effects of coverslip coating on adhesion and growth of urothelial carcinoma cells T24 and C3

For investigation of labelling of T24 and C3 cells by targeted nanoconjugates, these cells had to be seeded on coverslips in a well plate. Cell culturing plates with 24 wells (Costar) were chosen for this experiment. Glass coverslips with diameter of 13 mm were optimal for subsequent confocal fluorescent imaging. A choice of 13-mm coverslips included coated and uncoated. To investigate if T24 cells require coating of coverslips, they were seeded in a plate without coverslips, on non-coated glass coverslip, on crystal clear glass coverslips with Poly-D-lysine coating (NeuVitro) and on glass coverslip coated with Poly-D-lysine hydrobromide (Sigma) in our laboratory (**Figure 14**).

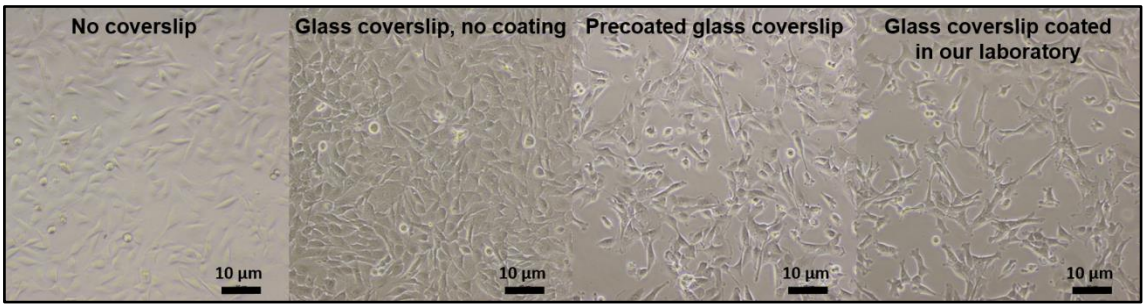

Figure 14. T24 cells growing in a 24-well plate without a coverslip, on a glass coverslip without coating, on a glass coverslip pre-coated with Poly-D-lysine and a coverslip coated with Poly-D-lysine in our laboratory.

The results suggested that the adhesion and growth of T24 cells on a glass coverslip without coating was sufficient and was not reduced in comparison with that of the coated coverslips. Coating of a coverslip in our laboratory had the same result as a pre-coated coverslip. The growth on the plastic surface in a well without a coverslip was found to be unsuitable for this experiment.

3.3.3. Optimal seeding density and fixation time point of T24 cells

To find optimal cell density for this experiment, we seeded 7.5×10^4, 1×10^5, 1.5×10^5, 2×10^5 and 2.5×10^5 cells per well on coverslips in a 24-well plate. Even though C3 were found to be smaller than T24 and could be seeded in a higher number of cells per well, we concluded that 2×10^5 cells per well is optimal to analyse luminescence from single cells. Less than 2×10^5 C3 cells would be challenging for a confocal fluorescent microscopy as not many cells could be observed in a field. More than 2×10^5 T24 cells per well was too many to analyse binding of nanoparticles to individual cells as some of them were too close to each other.

For the following investigation of targeted labelling, cells had to be fixed before incubation. To find the optimal time point for fixing, T24 and C3 cells were seeded on glass coverslips in a 24-well plate. Live cell imaging was then performed every 24 h for a few days. Optimal timing for fixing was found to be 24 h after seeding. This time was enough for the cells to adhere to the coverslips and was not enough for them to start dividing, which would be challenging for visualisation of single cells.

As a result of this experiment, we concluded that T24 and C3 cells for the investigation of targeted labelling should be seeded in the amount of 2×10^5 cells per well and fixed after 24 hours.

3.4. Conclusions

Urothelial carcinoma cells T24 and C3 were chosen to investigate their selective labelling by targeted upconversion photoluminescent nanoconjugates. T24 cell line demonstrated strong binding of MIL38 antibody, whereas binding of MIL38 to C3 cells was minimal. These results made T24 and C3 cell lines perfect candidates for the investigation of their targeted labelling by upconversion photoluminescent nanoconjugates. Analysis of their morphology, adhesion and growth allowed us to optimise their seeding for the following study. It was found that coating of coverslip does not improve adhesion and growth of these cell lines. The optimal seeding density was found to be 2×10^5 cells per well and the cells had to be fixed after 24 hours of incubation.

Chapter 4: Targeted labelling of urothelial carcinoma cells by photoluminescent nanoconjugates

4.1. Introduction

This chapter describes methodology and results of incubation of experimental and control nanoconjugates with T24 and C3 cells. Assessment of targeted binding of upconversion nanoconjugates UCNP@SiO_2-LPG-MIL38, was performed by incubation with Glypican-1 high T24 and Glypican-1 low C3 urothelial carcinoma cells. To find out the role of the antibody MIL38, other controls consisted of incubation of T24 cells with upconversion nanoconjugates UCNP@SiO_2-LPG-CRY104, functionalised by a control isotype cryptosporidium antibody CRY104 and with nanoconjugates UCNP@SiO_2-LPG, without an antibody. After the incubation, unbound nanoconjugates were washed away and confocal laser scanning microscopy was used to analyse the results. Visual quantification of labelled cells was followed by a computerised analysis of photoluminescence intensity of cells in all groups.

4.2. Materials and methods applied in the investigation of targeted labelling of urothelial carcinoma cells

4.2.1. Equipment for the analysis of targeted labelling of urothelial carcinoma cells

The imaging of labelled cells was performed by using a confocal laser-scanning microscope Zeiss LSM880 (Zeiss, Germany) equipped with 405-nm and 980-nm lasers, which allows detection of upconversion nanoconjugates on the cells. The laser with a wavelength 405-nm allowed visualisation of DAPI-stained nuclei and bright-field

imaging to visualise cell membranes. The 980-nm laser allows visualisation of upconversion nanoparticles. This microscope can perform Z-stack imaging of different layers and tile-scanning, which was useful in the analysis of a large number of cells. This microscope and ZEN imaging software were also used to analyse photoluminescence characteristics of labelled cells. Another innovative feature of this microscope is a superresolution mode termed Airyscan, where instead of a pinhole, a number of photodetectors were used creating a "synthetic aperture", affording the greater light collections efficiency and improved resolution. This mode was used in the preliminary experiments with UCNP and T24, however these results are not presented in this thesis.

4.2.2. Seeding of T24 and C3 cells to cell culture plates for the study of targeted labelling

The ability of targeted upconversion nanoconjugates UCNP@SiO_2-LPG-MIL38 to detect and label T24 urothelial carcinoma cells was studied *in vitro* by incubation of paraformaldehyde-fixed Glypican-1 high T24 and control Glypican-1 low C3 cells with UCNP@SiO_2-LPG-MIL38 nanoconjugates. Other controls were incubation of T24 cells with nanoconjugates UCNP@SiO_2-LPG-CRY104 with control antibody CRY104 and LPG-bound nanoconjugates not functionalised by any antibody UCNP@SiO_2-LPG. The optimisation steps of this experiment are described below.

For the labelling experiment, T24 and C3 cells were seeded into a cell culture plate at the density of 2×10^5 cells per well. In order to get this cell density, cells in 75-cm^2 cell culture flask were trypsinised by a 0.25 % Trypsin-EDTA solution, centrifuged and resuspended in 10-mL of RPMI 1640 media with 20% FBS. Then, 10-µL of cell suspension was mixed with 10-µL of trypan blue and applied into cell-counting chamber

slides, which was then inserted into an automated cell counter Countess C10281 (Invitrogen). Every cell counting procedure was performed at least twice.

T24 and C3 cells were seeded on glass coverslips in a 24-well plate. After incubation for 24 h at 37 ºC and 5% CO_2, cells were fixed with 4% PFA, which was prepared from methanol-free 16% Pierce Formaldehyde (Thermo Scientific) and PBS. Firstly, cells were washed three times by PBS. Then, 200-µL of 4% PFA was added to each well, cells were incubated at RT for 20 min. Then they were washed with PBS three more times and refrigerated for 24 h before the targeted labelling experiment.

4.2.3. Methodology of the incubation of T24 and C3 urothelial carcinoma cells with nanoconjugates

To find the lowest possible concentration of nanoconjugates, preliminary experiments included incubation of T24 and C3 cells with 500 µl per well of Tris buffer, containing 6.25, 12.5, 25, 37.5 or 50 µg of nanoconjugates. The minimal concentration of nanoconjugates suitable for our application was 12.5 µg of nanoconjugates per well.

Specific binding of targeted nanoconjugates UCNP@SiO_2-LPG-MIL38 was assessed *in vitro* by incubation with Glypican-1 high T24 and Glypican-1 low C3 urothelial carcinoma cells, which were fixed on glass coverslips in a 24-well plate. To investigate if the targeted binding of nanoconjugates was mediated by monoclonal antibodies MIL38, the other negative controls were set up. These included incubation of Glypican-1 positive T24 urothelial carcinoma cells with LPG bound upconversion nanoconjugates without functionalisation by an antibody (UCNP@SiO_2-LPG) and with upconversion nanoconjugates conjugated to a control isotype antibody CRY104 that did not have affinity towards urothelial carcinoma (UCNP@SiO_2-LPG-CRY104).

T24 and C3 cells were seeded on glass coverslips at the density of 2×10^5 cells per well, incubated for 24 h at 37º C with 5 % CO_2 and fixed for 20 min by a 4% PFA solution

Targeted upconversion nanoconjugates UCNP@SiO_2-LPG-MIL38, nanoconjugates UCNP@SiO_2-LPG-CRY104 functionalised by control antibodies CRY104 non-specific to Glypican-1, and nanoconjugates UCNP@SiO_2-LPG without antibodies were prepared in Tris-buffered saline. Their concentration was adjusted to 25 µg/mL and 500 µL of these solutions was added to the wells containing cells. Targeted nanoconjugates UCNP@SiO_2-LPG-MIL38 were added to T24 and C3 cells. Control nanoconjugates UCNP@SiO_2-LPG-CRY104 or UCNP@SiO_2-LPG, were added to the other wells containing T24 cells. After incubation for 1 h, coverslips were washed with PBS to remove unbound nanoconjugates. Then they were stained with nuclei staining DAPI and mounted on glass coverslips by using ProLong Diamond Antifade mountant with DAPI (Thermo Scientific) and sealed with nail polish for subsequent imaging using a confocal laser-scanning microscope and analysis of the sensitivity and specificity of *in vitro* labelling of T24 cells by targeted nanoconjugates UCNP@SiO_2-LPG-MIL38.

4.2.4. Methodology of confocal laser scanning microscopy of cells labelled by nanoconjugates

Zeiss LSM880 Confocal laser scanning microscope equipped with 405 and 980-nm lasers was used for imaging. For quantification of labelled cells and analysis of photoluminescence intensity, one coverslip was taken from each group and regions from 1.37 to 3.19 mm^2 were scanned in order to detect at least 110 cells in each group. An oil-immersion objective with 60× magnification and numerical aperture NA 1.4 was chosen for the imaging.

Images for analysis were obtained by using the maximum intensity projection of stack images in order to detect all nanoparticles from the bottom to the top edge of every cell (**Figure 15, A**). Three channels were used during laser-scanning confocal microscopy (**Figure 15, B-E**). The first channel was used to observe upconversion nanoconjugates, detecting light in the range of 495-634 nm under the illumination with a 980-nm laser (**Figure 15, B**). The second channel was used to detect DAPI stained cell nuclei and was tuned to acquire 410-495-nm light under the illumination with a 405-nm laser (**Figure 15, C**). The third channel used transmitted 405-nm light to obtain bright-field images, in order to see the cell membrane and edges of cells (**Figure 15, D**).

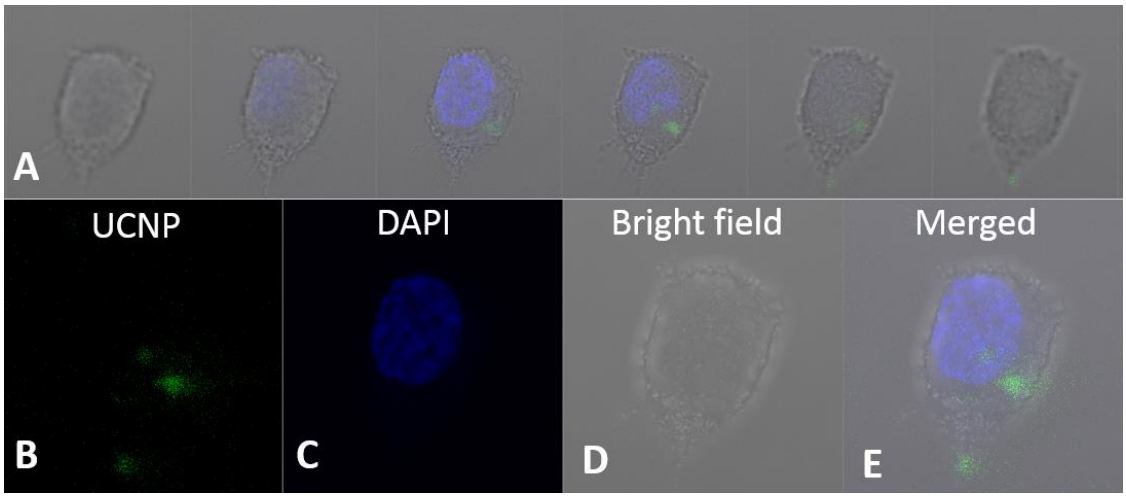

Figure 15. Stack images of T24 cell after incubation with UCNP@SiO_2-LPG-MIL38 **(A)** and its maximum intensity projection split into three channels: UCNP **(B)**, DAPI **(C)**, bright field image **(D)**; and merged image **(E).** Magnification 60×.

4.2.5. Methodology of the analysis of targeted labelling

As a result of the laser-scanning confocal microscopy, we obtained images of 127 T24 cells, incubated with UCNP@SiO_2-LPG-MIL38, 111 T24 cells incubated with

UCNP@SiO_2-LPG-CRY104, 130 cells incubated with UCNP@SiO_2-LPG and 112 C3 cells incubated with UCNP@SiO_2-LPG-MIL38.

Firstly, cells were visually classified as labelled with nanoconjugates and non-labelled and their proportions were calculated. Then, proportions of the labelled cells were compared between the groups to determine the sensitivity and specificity of the binding of targeted upconversion photoluminescent nanoconjugates UCNP@SiO_2-LPG-MIL38 to T24 and C3 urothelial carcinoma cells.

Secondly, computer analysis was performed to compare the photoluminescence intensity of T24 and C3 cells after incubation with nanoconjugates. Using imaging software ZEN, every single cell was manually contoured as a region of interest to detect the photoluminescence intensity from nanoconjugates bound to each cell (**Figure 16**). The cell membrane visualisation by transmitted light was used to contour each cell as a region of interest, in order to analyse the intensity of light in each channel coming from a single cell. Mean intensity of upconversion photoluminescence was then measured in every single cell in each treatment group by using ZEN software. Then the photoluminescence intensity of cells was compared between groups.

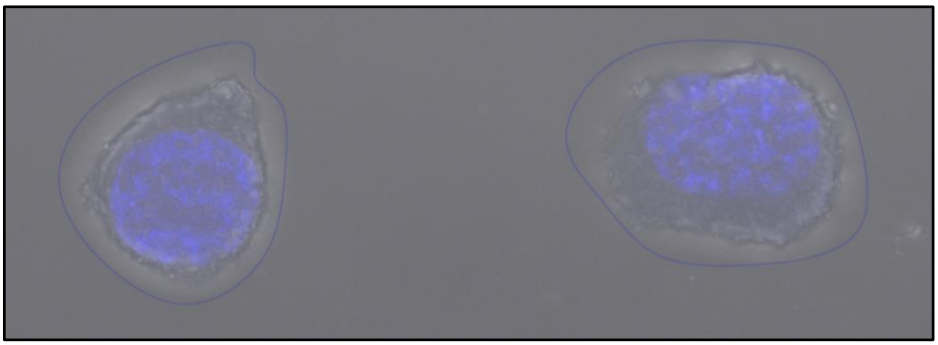

Figure 16. Example of manual selection of a cell as a region of interest using Carl Zeiss proprietary imaging software ZEN (blue line). Magnification 60×.

4.3. Results of the experimental study of targeted labelling of urothelial carcinoma cells

4.3.1. Results of visual analysis of confocal microscopy images

Specific binding of the targeted upconversion nanoconjugates UCNP@SiO_2-LPG-MIL38 was assessed *in vitro* by incubation with Glypican-1 positive T24 and Glypican-1 negative C3 urothelial carcinoma cells fixed on glass coverslips in wells of a 24-well plate.

To demonstrate that the targeted binding of nanoconjugates was mediated by a monoclonal antibody MIL38, the other negative controls included incubation of T24 urothelial carcinoma cells with nanoconjugates UCNP@SiO_2-LPG, without functionalisation by an antibody and with nanoconjugates UCNP@SiO_2-LPG-CRY104 coupled to control isotype antibodies that should not have affinity towards urothelial carcinoma cells.

The microscopy imaging demonstrated binding of the targeted nanoconjugates functionalised by a Glypican-1 monoclonal antibody MIL38 to the vast majority of T24 cells (**Figure 17, A**). Labelled cells were easily observable due to the upconversion photoluminescence originated from upconversion nanoparticles under illumination by a 980-nm laser, which was not affected by the conjugation with MIL38 antibodies.

In contrast, only few Glypican-1 low C3 cells were labelled by UCNP@SiO_2-LPG-MIL38 and even non-specifically labelled cells had the lower intensity of the photoluminescence than T24 cells (**Figure 17, B**).

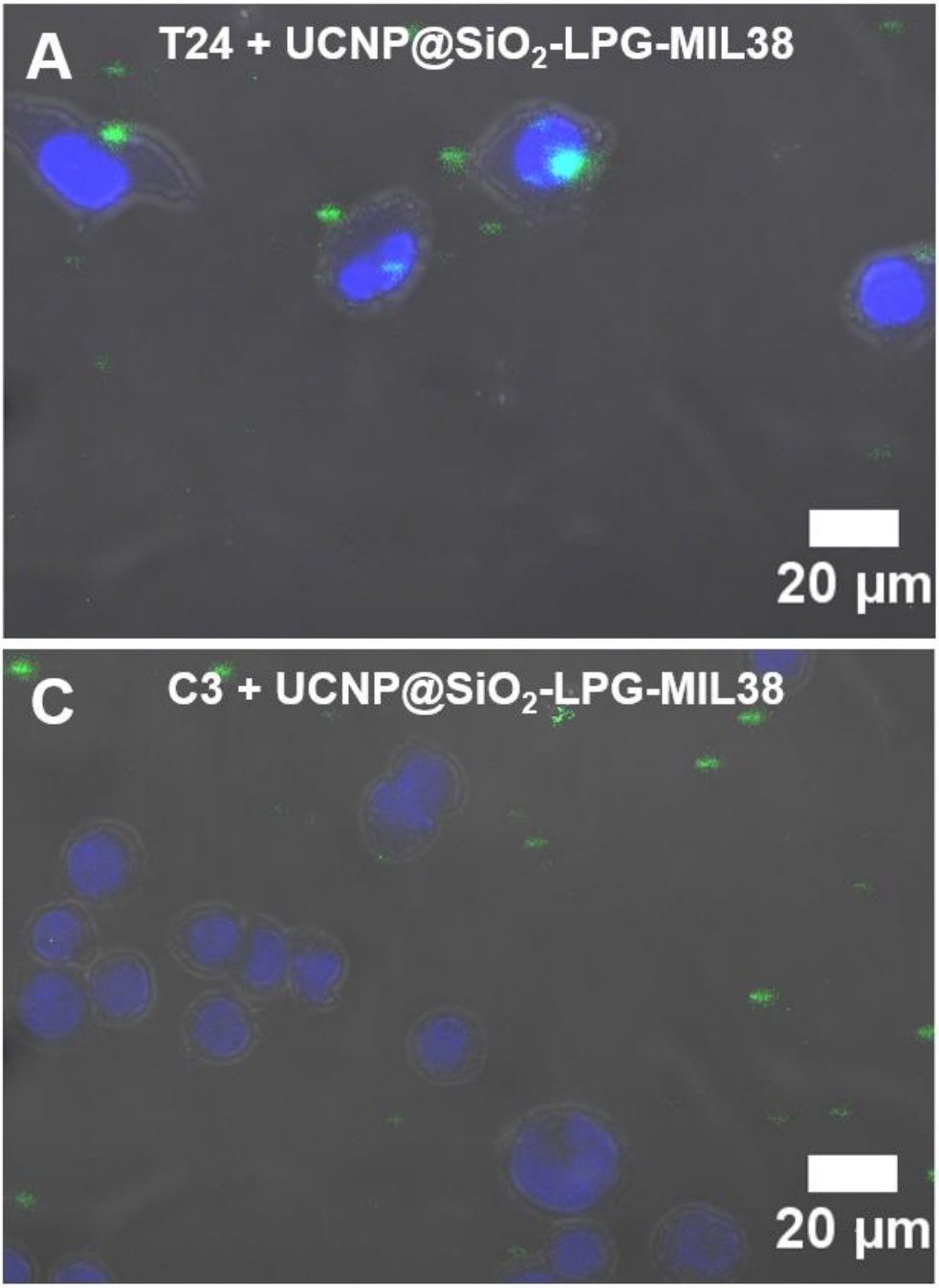

Figure 17. Glypican-1 positive T24 (A) and Glypican-1 negative C3 (Bottom) urothelial carcinoma cells incubated with UCNP@SiO_2-LPG-MIL38 nanoconjugates. Merged images of 3 channels, detecting UCNP (green), DAPI (blue) and bright-field. Magnification 60×.

Incubation of T24 cells with UCNP@SiO_2-LPG-CRY104 and UCNP@SiO_2-LPG also resulted in only few cells being labelled (**Figure 18**).

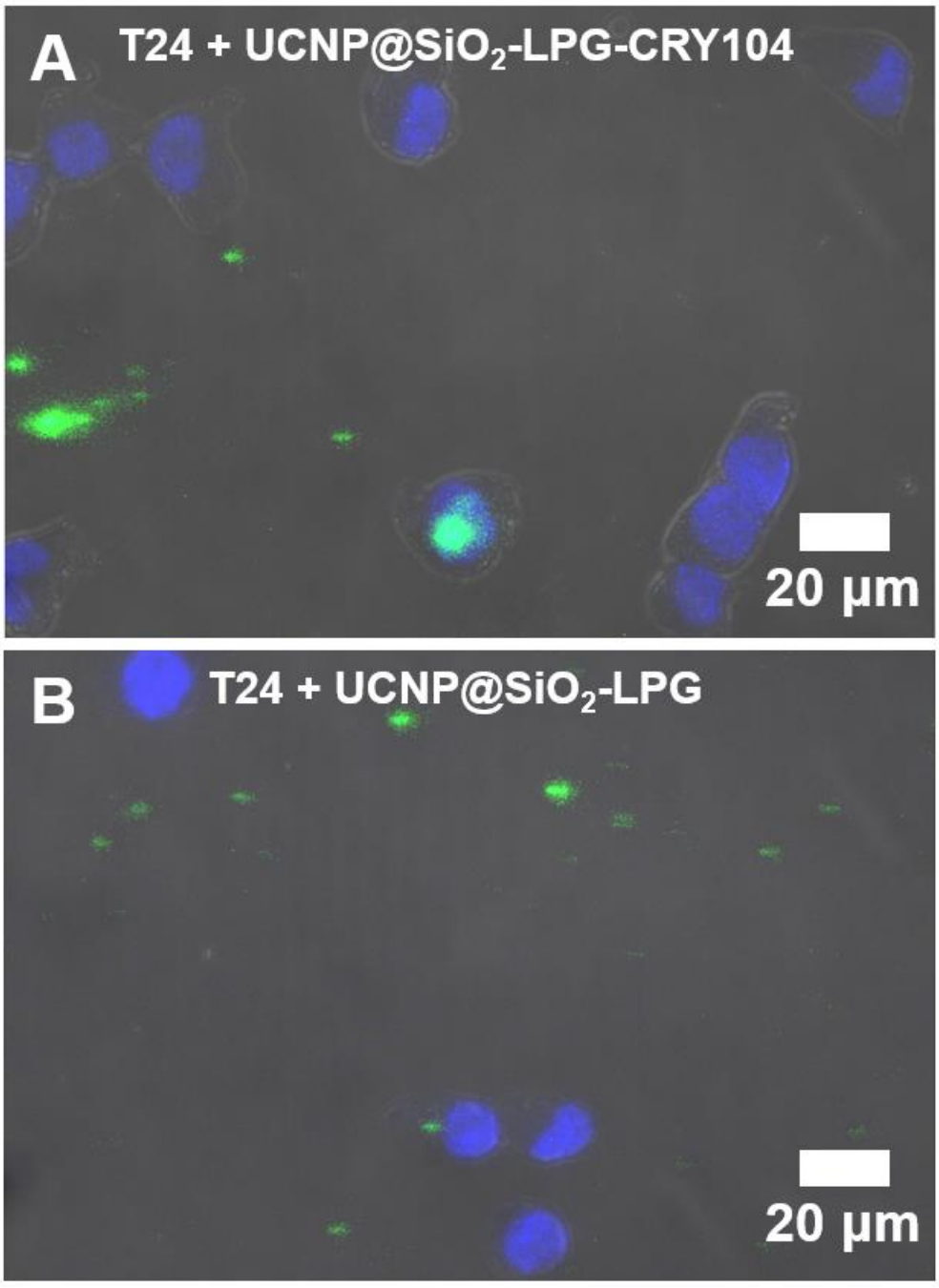

Figure 18. Control T24 urothelial carcinoma cells incubated with nanoconjugates UCNP@SiO_2-LPG-CRY104 (**A**) or UCNP@SiO_2-LPG (**B**). Merged images of 3 channels, detecting UCNP (green), DAPI (blue) and bright-field. Magnification 60×.

Upconversion nanoconjugates were observable in all groups, although they were predominantly found adhered to the plate (perceived as background) rather than on the cells in the control groups. **Figure 19** shows results of the incubation separated into different channels showing UCNP, cell nuclei (DAPI), bright-field and merged images for comparison between experimental groups.

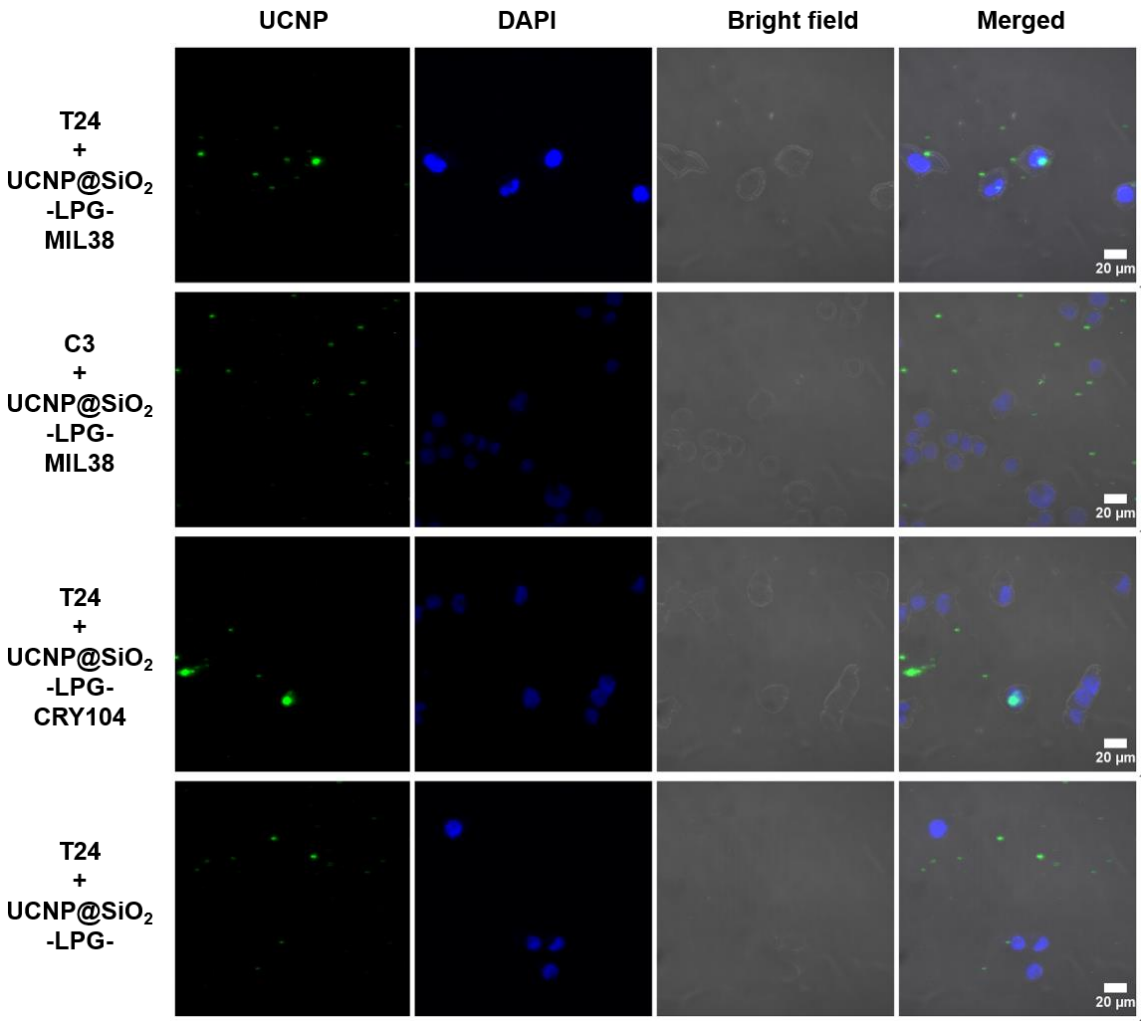

Figure 19. Microscopy laser-scanning confocal fluorescence images of T24 and C3 cells incubated with targeted nanoconjugates UCNP@SiO_2-LPG-MIL38 (First and Second rows); T24 cells incubated with nanoconjugates UCNP@SiO_2-LPG-CRY104 (Third row) and UCNP@SiO_2-LPG (Forth row), Magnification 60×.

4.3.2. Results of visual quantification of labelled cells

One coverslip from each experimental group was taken for visual quantification of the labelled cells. Confocal laser-scanning microscopy of regions from 1.37 to 3.19 mm^2 was performed at 60× magnification to detect a representative number of cells in each group. It resulted in imaging of 127 T24 cells, incubated with UCNP@SiO_2-LPG-MIL38, 111 T24 cells incubated with UCNP@SiO_2-LPG-CRY104, 130 T24 cells incubated with UCNP@SiO_2-LPG and 112 C3 cells incubated with UCNP@SiO_2-LPG-MIL38. Visual analysis was then performed to separate cells within each treatment group into those labelled with nanoconjugates and unlabelled, and calculate their proportions. Finally, the proportions of the labelled cells were compared between the groups.

Out of 127 T24 cells incubated with targeted upconversion photoluminescent nanoconjugates UCNP@SiO_2-LPG-MIL38, 111 cells were labelled by targeted upconversion nanoconjugates, making up almost 90% of the entire cell population.

The incubation of the same nanoconjugates with the control C3 cells resulted in labelling of only 23.2%, which was probably caused by the low expression of Glypican-1. Among the T24 cells incubated with nanoconjugates with the control antibodies (UCNP@SiO_2-LPG-CRY104) and incubated with nanoconjugates without antibodies (UCNP@SiO_2-LPG), only 22 and 34 cells were labelled, making up 19.8 % and 26.2 % of the entire cell population, respectively. MIL38 caused specific binding of at least 61.2% in the targeted group, as up to 26.2% might have been non-specific.

These results proved the specificity of the binding of the targeted nanoconjugates UCNP@SiO_2-LPG-MIL38, which predominantly bound to Glypican-1 positive T24 cells. This specificity was found to be caused by a Glypican-1 monoclonal antibody

MIL38, as nanoconjugates without this antibody or with a control isotype antibody CRY104 did not bind to T24 cells at the same level. This result shows that MIL38 antibody has a high potential in targeted delivery of biohybrid nanocompounds to T24 urothelial carcinoma cells and other cells expressing Glypican-1. The results of the visual quantification of the labelled cells are presented in **Figure 20**.

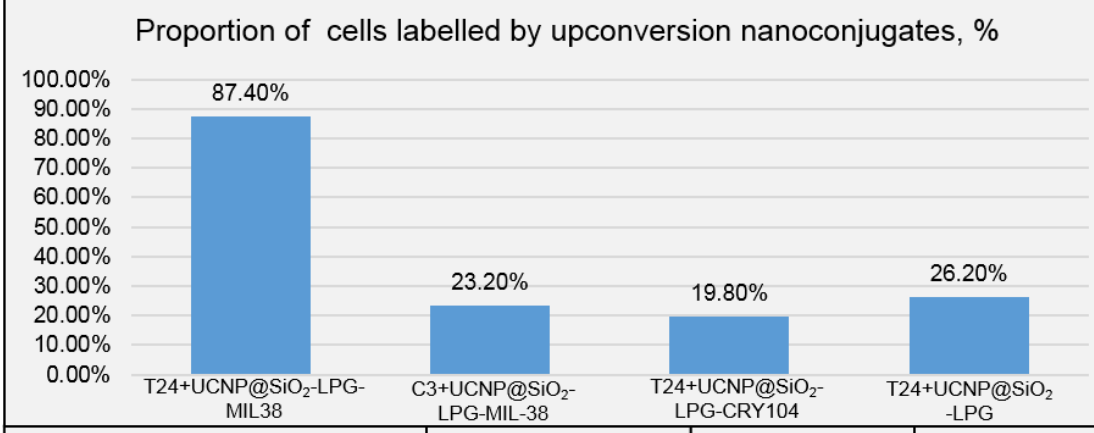

Treatment group	Number of cells labelled by UCNP	Total number of cells	Proportion of labelled cells
T24 + UCNP@SiO_2-LPG-MIL38	111	127	87.4 %
C3 + UCNP@SiO_2-LPG-MIL-38	26	112	23.2 %
T24 + UCNP@SiO_2-LPG-CRY104	22	111	19.8 %
T24 + UCNP@SiO_2-LPG	34	130	26.2 %

Figure 20. A bar chart and a table illustrating the percentage of Glypican-1 high T24 and Glypican-1 low C3 urothelial carcinoma cells labelled by targeted nanoconjugates UCNP@SiO_2-LPG-MIL38 and T24 cells labelled by nanoconjugates UCNP@SiO_2-LPG-CRY104 or UCNP@SiO_2-LPG, n = 1. The table also shows the number of labelled cells and the total number of cells, observed in experimental and control groups.

4.3.3. Results of the analysis of the intensity of photoluminescence of cells in different groups

In addition to the visual analysis of the binding specificity, the labelling performance was also characterised by measuring the photoluminescence intensity of cells in different groups after incubation with photoluminescent nanoconjugates. Photoluminescence intensity from the total of 480 cells from different groups was measured and compared between the groups, further demonstrating significance of the selectivity and labelling ability of the targeted upconversion nanoconjugates UCNP@SiO_2-LPG-MIL38 (**Table 2**; **Figure 21**).

The mean photoluminescence intensity of all T24 cells incubated with nanoconjugates UCNP@SiO_2-LPG-MIL38 was found to be almost eight times higher than the mean photoluminescence intensity of C3 cells incubated with the same nanoconjugates and was more than five times higher than mean photoluminescence intensity of T24 cells incubated with control nanoconjugates UCNP@SiO_2-LPG-CRY104 or UCNP@SiO_2-LPG (**Table 2**; **Figure 21**).

Table 2. Mean photoluminescence intensity and standard error of T24 and C3 cells incubated with UCNP@SiO_2-LPG-MIL38 and T24 cells incubated with UCNP@SiO_2-LPG-CRY104 or UCNP@SiO_2-LPG, p = 0.05.

	T24 + UCNP@SiO_2-LPG-MIL38	C3 + UCNP@SiO_2-LPG-MIL38	T24 + UCNP@SiO_2-LPG-CRY104	T24 + UCNP@SiO_2-LPG
Mean photoluminescence intensity, a.u.	0.346 ± 0.038	0.045 ± 0.004	0.045 ± 0.020	0.065 ± 0.012

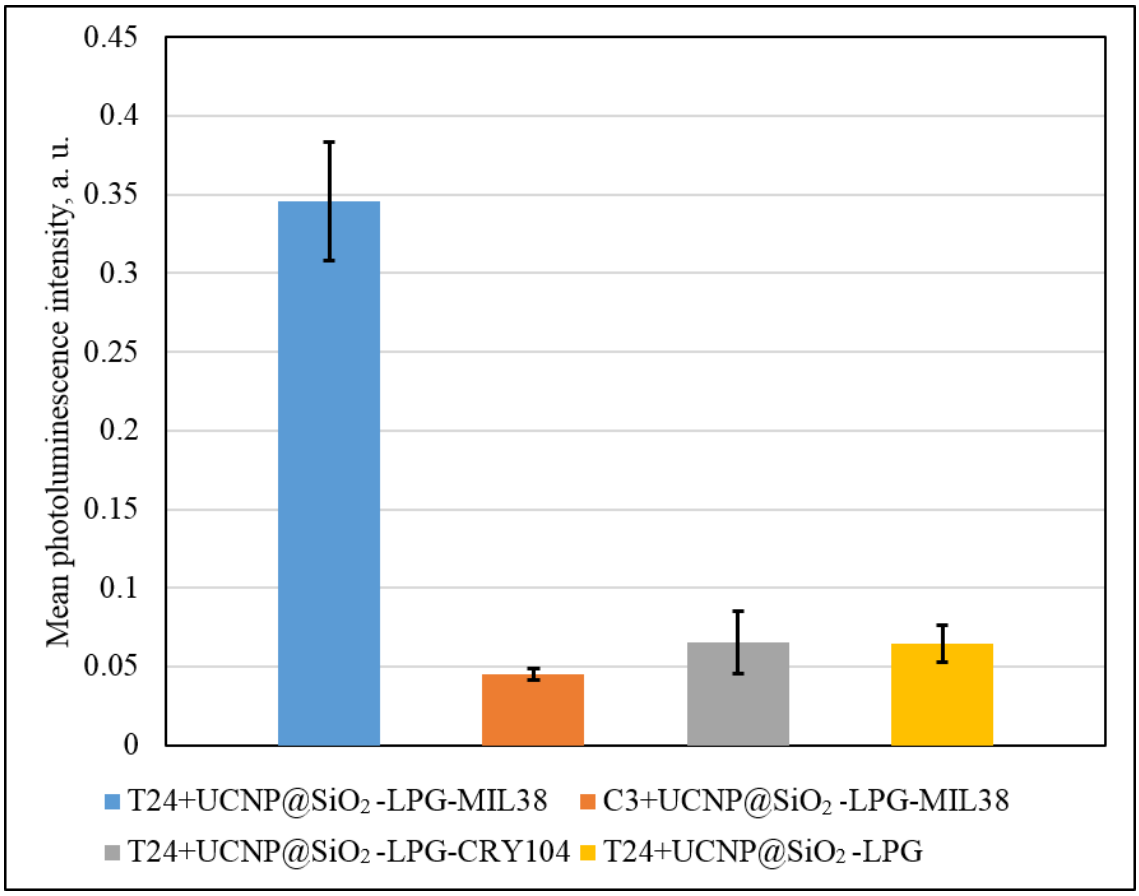

Figure 21. Bar chart showing mean photoluminescence intensity of T24 and C3 cells incubated with UCNP@SiO_2-LPG-MIL38, T24 cells incubated with UCNP@SiO_2-LPG-CRY104 and T24 cells incubated with UCNP@SiO_2-LPG. Error bars represent the 95% confidence interval of the mean.

Such a significant difference in the photoluminescence intensity of cells from the tested groups further demonstrated considerable potential of upconversion photoluminescent nanoconjugates UCNP@SiO_2-LPG-MIL38 for targeting and binding to T24 urothelial carcinoma cells. It also proved applicability of upconversion nanoparticles for photoluminescent labelling and highlighted potential of these nanoconjugates for applications in photodynamic diagnosis and therapy of bladder cancer.

4.4. Conclusions

Incubation of T24 and C3 cells with the targeted photoluminescent nanoconjugates resulted in targeted labelling of the majority of T24 cells. Analysis of the images concluded that 87.4% of T24 cells were labelled. The analysis of the photoluminescence intensity in different groups further confirmed the effectivity of targeted upconversion photoluminescent nanoconjugates UCNP@SiO_2-LPG-MIL38 in labelling T24 cells, as their photoluminescence was up to eight times greater than that of the control groups. It was also proven that the targeting of these nanoconjugates was strongly dependent on a monoclonal antibody MIL38.

Chapter 5: Discussion, Conclusions and Future Directions

5.1. Discussion of the techniques applied in this study

This project studied potential of the targeted upconversion photoluminescent nanoconjugates representing upconversion nanoparticles coupled to antibodies for photodynamic diagnosis and therapy of bladder cancer.

PDD and PDT of bladder cancer show considerable promise in bladder cancer treatment, as they can act at the causes of its recurrence and progression. However, the existing photosensitisers are associated with a number of adverse side effects, have low specificity and their treatment depth is limited to superficial layers of tumours. They also suffer from inability of proper targeting and adjustment of therapeutic effect. Biohybrid photoluminescent nanoconjugates based on the upconversion nanoparticles are promising for solving the problem of the greater treatment depth by using near-infrared light to photoactivate photosensitisers. This can lead to the reduction of recurrence and progression rates. Moreover, linked with different therapeutic agents and different antibodies, upconversion nanoconjugates capable to carry photosensitiser and other drugs to combine different modalities of action on cancer cells optimised for each patient.

In this experiment, upconversion nanoparticles were conjugated with anti-Glypican-1 monoclonal antibodies MIL38 to target urothelial carcinoma cells T24. Other methods of tumour targeting by nanoparticles include passive targeting by enhanced permeability and retention (EPR-effect) of tumours and active targeting by folic acid or peptides, which are going to be discussed in the following paragraphs[169].

In 1986, Matsumura and Hiroshi Maeda observed enhanced accumulation of macromolecules in a tumour[170]. This phenomenon was then called EPR-effect, which is caused by specificity of tumour vasculature, leading to accumulation of macromolecules and nanoparticles[171]. The main advantage of this passive targeting is that injected intravenously nanoparticles of size 400 nm and under can accumulate in a tumour without any specific targeting agents. The disadvantage is that such delivery is possible only in relatively large tumours with developed vasculature and is not effective against small tumours and metastases. Another shortfall of this method is related to the passive transport inability to promote cellular uptake of extravasated nanoparticles, which is critical for some applications. In tumours of the urinary bladder, passive accumulation of nanoparticles in larger tumours may be possible, but would be limited to a systemic intravenous injection and would not be suitable for intravesical instillation, which is important to avoid systemic absorption and adverse effects in normal tissues and organs.

Active targeting of nanoparticles is usually based on an antibody, antibody fragments, aptamers or ligand-based targeting[172]. Binding to an antibody was the first and widespread approach of targeting nanoparticles[173]. In comparison with the other methods, antibodies do not require modification and are amenable for easy conjugation using a number of protocols. One of the noteworthy protocols based on LPG linker ensures facile and universal attachment of antibody to all types of nanoparticles surface-coated with a silica layer. The presence of fragments with different functions in an antibody allows oriented coupling to a nanoparticle, where Fc fragment binds to a nanoparticle and Fab fragments remain available for binding to a specific antigen. As such, the oriented binding provides high efficacy and low risk of aggregation, which is oftentimes caused by binding of a single antibody molecule to several nanoparticles.

We produced upconversion nanoparticles amenable for conjugation with biomolecules. These nanoparticles had an average diameter of 33.1 ± 1.5 nm and exhibited upconversion photoluminescence. They were coated with a layer of silica and functionalised by LPG linker to be able to bind to a variety of Ig-G antibodies. The method of the production of upconversion nanoparticles appeared to be effective and yielded nanoparticles with desired shape, size and upconversion photoluminescence intensity. Coating with silica is a well-known and widely applied approach of the surface-modification of upconversion nanoparticles[139,174,175]. In addition to an opportunity to load drugs onto a nanoparticle, a number of studies applied silica-coated upconversion nanoparticles as nanocarriers with a remote-controlled release[141,142]. We used the silica-coating to apply LPG-mediated conjugation of upconversion nanoparticles with MIL38, following a previously published protocol, which was developed by Care *et al.*[144] and also applied in our laboratory by Liang *et al.*[137]. This protocol was found to be highly efficient and non-laborious, as the loss of nanoparticles and antibodies was minimal and conjugated antibodies had their Fab fragments available for binding to their antigens[137].

Incubation of urothelial carcinoma cells T24 and C3 with nanoconjugates revealed their ability to target Glypican-1 positive cells. It also demonstrated the role of MIL38 in targeted labelling. This *in vitro* study is a necessary step before further *in vivo* investigation of viability of this technique for PDD and PDT of bladder cancer.

5.2. Significance of the results and potential applications

The incubation of urothelial carcinoma cells T24 with targeted nanoconjugates UCNP@SiO_2-LPG-MIL38 resulted in labelling of 87.4% of cells and photoluminescence of targeted cells with the intensity up to eight times higher than in the control groups.

These findings demonstrated specific targeted labelling of T24 cells by targeted nanoconjugates UCNP@SiO_2-LPG-MIL38. Moreover, a series of control experiments demonstrated that specificity of this photoluminescent labelling was provided by MIL38 monoclonal antibody. These results demonstrating the high sensitivity and specificity of upconversion nanoconjugates functionalised by MIL38 suggests that these nanoconjugates have a great potential in fluorescence cystoscopy, fluorescence-guided resection and PDT of bladder cancer.

5.2.1. Potential application in bladder cancer diagnosis

In fluorescence cystoscopy and fluorescence-guided resection of bladder tumour, one of the main advantages of these nanoconjugates would be their targeting properties. Sensitivity and specificity of conventional sensitizers, such as 5-ALA and hexaminolevulinate, are based on slight metabolic differences between normal and cancer cells. It leads to their non-specific accumulation and labelling of inflamed or, sometimes, even normal bladder urothelium and inconsistent sensitivity caused by high variability of bladder tumours. In contrast, antibody-functionalised nanoconjugates can target specific antigens, expressed by cancer cells, regardless of their metabolic state. In particular, MIL38 demonstrated strong affinity towards a Glypican-1 positive urothelial carcinoma cell line. However, discovery of other antigens expressed by bladder cancer would allow conjugation of targeted nanoconjugates with other antibodies. Another advantage of targeted upconversion nanoconjugates for PDD is upconversion of near-infrared into visible light. This means that the bladder wall will need to be illuminated by deep-penetrating invisible 980-nm light to induce visible photoluminescence of the nanoconjugates. It will result in a background-free green photoluminescence of cancer cells, whereas the illumination of bladder walls with visible and UV light poses

challenges in suspicious lesion imaging and visualisation due to the eclipsing background due to tissue autofluorescence and strong scattering.

5.2.2. Potential application in bladder cancer therapy

Another envisaged application of these nanoconjugates is therapy of bladder cancer. Here, molecular targeting is also important to avoid undesirable accumulation of cytotoxic drugs in healthy bladder wall or other organs. As mentioned previously, nanoconjugates developed in this project can act as nanocarriers for a variety of molecules with remote-controlled release by deep-penetrating near-infrared laser, so that a cytotoxic drug is released only when and where needed. Thus, nanoconjugates have a potential in targeted chemo and genetic therapy of bladder cancer. After accumulation in a tumour, nanoconjugates could release drugs in response to deep-penetrating near-infrared illumination, which would be possible in the bladder, due to the convenience of transurethral endoscopic access.

For PDT, targeted upconversion nanoconjugates could also act as remote-controlled nanotransducers and a photosensitiser carrier for photodynamic therapy[176]. Such complex photodynamic agents have a great potential as they can overcome a number of limitations inherent to conventional photosensitisers. Firstly, they can significantly increase the treatment depth, by converting a deep-penetrating near-infrared light into a high-energy visible light. This conversion can be followed by a highly efficient activation of a photosensitiser, as the photosensitiser can be incorporated into the silica layer and be in a proximity to the upconversion nanoparticle[137,138]. Secondly, they can combine photodynamic therapy with other modalities. For example, in addition to a photosensitiser, lanthanide-doped upconversion nanoparticles were previously coupled

with Gadolinium for multimodal MRI/photoluminescent imaging and PDT[125,177] and were used for multimodal photothermal/photodynamic therapy[178,179]. In 2014, Fan, *et al*. have reported the production and application of upconversion nanoparticles-based nanocomplexes for a bimodal MRI/photoluminescent imaging and a tri-modal chemo-/radio-/photodynamic therapy, achieving good results in the elimination of a tumour *in vivo*[124]. The importance of the targeted multimodal action on tumours and metastases was also recently highlighted by Steeg[169]. The targeted upconversion photoluminescent nanoconjugates produced in this project also present multifunctional agents and their multimodality can be further expanded through their modification.

5.3. Limitations of this research project

This investigation of targeted labelling of urothelial carcinoma cells had a number of limitations. The main limitation is that this study was performed on fixed cells. Fixed cells were chosen to investigate if there was specificity in the binding of these nanoconjugates to urothelial carcinoma cells. Live cells experiment would give a better understanding of the behaviour of nanoconjugates in physiological conditions, although would be more complicated and potentially require much time for optimisation of the experiment. The experiment with fixed cells was a proof-of-concept and demonstrated the selective binding of functional nanoconjugates and their photoluminescence, showing their potential for future studies.

Another limitation of this project was the lack of experiments using normal bladder cells. Our study demonstrated that targeted upconversion nanoconjugates coupled to MIL38 can distinguish between different urothelial carcinoma cell lines. This work should be extended to normal bladder cells to further assess the specificity of the

nanoconjugates and their potential for diagnosis and therapy of bladder cancer. This is a crucial next step, as binding to a normal bladder is the main issue, currently associated with fluorescent cystoscopy.

Another major limitation of this study is that it is yet unknown how these targeted nanoconjugates will behave in a living organism, including their colloidal stability, circulation time, clearance pathways and ability to target bladder tumour after intravenous or intravesical instillation.

The next limitation of this study was that only one coverslip from each group was used for the final quantification of cells labelled by targeted upconversion nanoconjugates and for the analysis of mean photoluminescent intensity. However, the consistency of specific labelling of T24 cells was observed in all preliminary experiments. Furthermore, it was a proof-proof-concept study, where our aim was to investigate the possibility of the production of target upconversion nanoconjugates coupled to a MIL38 antibody and to detect any specificity in their binding to urothelial carcinoma cells T24 with high expression of Glypican-1.

Finally, nonspecific binding and aggregation are currently among the main limitations of described targeted upconversion nanoconjugates, as specificity of labelling is crucial for clinical applications. While this non-specific binding can be caused by the nanoparticle and by LPG linker, conjugation of antibody does not seem to increase it. Coating of nanoparticles with a layer of silica reduces their aggregation and non-specific binding. However, it can be further improved by several methods. Carboxylate, amine, polyethylene glycol, and octadecyl and other functional groups on the surface of nanoparticles can improve their specificity and colloidal stability[180]. Effect of various

surface modification on aggregation and specificity of binding will be studied in the following experiments.

5.4. Conclusions

In this study, we demonstrated the production of targeted upconversion photoluminescent nanoconjugates UCNP@SiO_2-LPG-MIL38 for photodynamic diagnosis and therapy of bladder cancer and assessed their selectivity and molecular specificity towards Glypican-1 positive urothelial carcinoma cells T24. These nanoconjugates labelled almost 90% of targeted cells and made them observable upon the excitation with a near-infrared laser. This is a significant result, showing a high potential of these nanoconjugates for further exploration of PDT and PDD. It was found that the monoclonal antibody MIL38 holds promise for diagnosis, drug delivery and targeted therapy, as it mediated the targeted binding of upconversion photoluminescent nanoconjugates to Glypican-1 positive urothelial carcinoma cells.

5.5. Future directions

Our future directions include investigation of intracellular uptake of nanoconjugates UCNP@SiO_2-LPG-MIL38 by live T24 and primary normal bladder cells. These cell lines are planned to be co-cultured and incubated with nanoconjugates. The multiplexing ability of nanoconjugates, as well as their intracellular uptake and distribution will be studied. The study involving normal bladder cells is necessary to analyse the specificity of the nanoconjugates and assess their potential effects on healthy urinary bladder wall.

Then, we plan to perform a series of *in vivo* experiments, involving intravesical instillation of targeted nanoconjugates UCNP@SiO_2-LPG-MIL38 to rats bearing orthotopic xenograft of a bladder tumour to further study application of targeted upconversion photoluminescent nanoconjugates for detection and therapy of bladder tumours. These experiments will demonstrate behaviour of upconversion nanoconjugates in physiological conditions and allow for a comprehensive assessment of their toxicity.

Another direction of future studies is investigation of the expression of the proteoglycan Glypican-1 in bladder tumours resected from patients. That study will investigate role of Glypican-1 in recurrence and progression and assess the possibility of its application for prognosis of bladder cancer. Moreover, it will further demonstrate applicability of nanoconjugates linked with a monoclonal antibodies MIL38 for diagnosis and therapy of bladder cancer.

References

1 Siegel, R. L., Miller, K. D. & Jemal, A. Cancer statistics, 2016. *CA Cancer J Clin* **66**, 7-30, doi:10.3322/caac.21332 (2016).

2 Yeung, C., Dinh, T. & Lee, J. The health economics of bladder cancer: an updated review of the published literature. *PharmacoEconomics* **32**, 1093-1104, doi:10.1007/s40273-014-0194-2 (2014).

3 Ferlay, J. *et al.* Cancer incidence and mortality worldwide: sources, methods and major patterns in GLOBOCAN 2012. *International Journal of Cancer. Journal International du Cancer* **136**, E359-386, doi:10.1002/ijc.29210 (2015).

4 Botteman, M. F., Pashos, C. L., Redaelli, A., Laskin, B. & Hauser, R. The health economics of bladder cancer: a comprehensive review of the published literature. *PharmacoEconomics* **21**, 1315-1330 (2003).

5 Svatek, R. S. *et al.* The economics of bladder cancer: costs and considerations of caring for this disease. *European Urology* **66**, 253-262, doi:10.1016/j.eururo.2014.01.006 (2014).

6 Green, D. A. *et al.* Cost-effective treatment of low-risk carcinoma not invading bladder muscle. *BJU International* **111**, E78-84, doi:10.1111/j.1464-410X.2012.11454.x (2013).

7 Sievert, K. D. *et al.* Economic aspects of bladder cancer: what are the benefits and costs? *World Journal of Urology* **27**, 295-300, doi:10.1007/s00345-009-0395-z (2009).

8 Burger, M. *et al.* Epidemiology and risk factors of urothelial bladder cancer. *European Urology* **63**, 234-241, doi:10.1016/j.eururo.2012.07.033 (2013).

9 Rafnar, T. *et al.* European genome-wide association study identifies SLC14A1 as a new urinary bladder cancer susceptibility gene. *Hum Mol Genet* **20**, 4268-4281, doi:10.1093/hmg/ddr303 (2011).

10 Gu, J., Liang, D., Wang, Y., Lu, C. & Wu, X. Effects of N-acetyl transferase 1 and 2 polymorphisms on bladder cancer risk in Caucasians. *Mutat Res* **581**, 97-104, doi:10.1016/j.mrgentox.2004.11.012 (2005).

11 Sobti, R. C. *et al.* Genetic polymorphisms of CYP2D6, GSTM1, and GSTT1 genes and bladder cancer risk in North India. *Cancer Genet Cytogenet* **156**, 68-73, doi:10.1016/j.cancergencyto.2004.04.001 (2005).

12 Freedman, N. D., Silverman, D. T., Hollenbeck, A. R., Schatzkin, A. & Abnet, C. C. Association between smoking and risk of bladder cancer among men and women. *JAMA* **306**, 737-745, doi:10.1001/jama.2011.1142 (2011).

13 Purdue, M. P. & Silverman, D. T. Clearing the Air: Summarizing the Smoking-related Relative Risks of Bladder and Kidney Cancer. *European Urology* **70**, 467-468, doi:10.1016/j.eururo.2016.04.009 (2016).

14 Ghadimi, T., Gheitasi, B., Nili, S., Karimi, M. & Ghaderi, E. Occupation, smoking, opium, and bladder cancer: A case-control study. *South Asian J Cancer* **4**, 111-114, doi:10.4103/2278-330X.173174 (2015).

15 Cumberbatch, M. G., Cox, A., Teare, D. & Catto, J. W. Contemporary Occupational Carcinogen Exposure and Bladder Cancer: A Systematic Review and Meta-analysis. *JAMA Oncol* **1**, 1282-1290, doi:10.1001/jamaoncol.2015.3209 (2015).

16 Bellmunt, J. *et al.* Bladder cancer: ESMO Practice Guidelines for diagnosis, treatment and follow-up. *Annals of oncology : official Journal of the European Society for Medical Oncology / ESMO* **25 Suppl 3**, iii40-48, doi:10.1093/annonc/mdu223 (2014).

17 Witjes, J. A. *et al.* EAU guidelines on muscle-invasive and metastatic bladder cancer: summary of the 2013 guidelines. *European Urology* **65**, 778-792, doi:10.1016/j.eururo.2013.11.046 (2014).

18 Babjuk, M. *et al.* EAU guidelines on non-muscle-invasive urothelial carcinoma of the bladder: update 2013. *European Urology* **64**, 639-653, doi:10.1016/j.eururo.2013.06.003 (2013).

19 Hall, M. C. *et al.* Guideline for the management of nonmuscle invasive bladder cancer (stages Ta, T1, and Tis): 2007 update. *The Journal of Urology* **178**, 2314-2330, doi:10.1016/j.juro.2007.09.003 (2007).

20 Grossfeld, G. D. *et al.* Asymptomatic microscopic hematuria in adults: summary of the AUA best practice policy recommendations. *Am Fam Physician* **63**, 1145-1154 (2001).

21 Maclennan, S. J. *et al.* Urological cancer care pathways: development and use in the context of systematic reviews and clinical practice guidelines. *World Journal of Urology* **29**, 291-301, doi:10.1007/s00345-011-0660-9 (2011).

22 Brausi, M. *et al.* A review of current guidelines and best practice recommendations for the management of nonmuscle invasive bladder cancer by the International Bladder Cancer Group. *J Urol* **186**, 2158-2167, doi:10.1016/j.juro.2011.07.076 (2011).

23 Babjuk, M. *et al.* EAU Guidelines on Non-Muscle-invasive Urothelial Carcinoma of the Bladder: Update 2016. *European Urology*, doi:10.1016/j.eururo.2016.05.041 (2016).

24 Murphy, W. M., Busch, C. & Algaba, F. Intraepithelial lesions of urinary bladder: morphologic considerations. *Scand J Urol Nephrol Suppl*, 67-81 (2000), doi:10.1080/003655900750016922-1

25 Martin, F. M. & Kamat, A. M. Definition and management of patients with bladder cancer who fail BCG therapy. *Expert Review of Anticancer Therapy* **9**, 815-820, doi:10.1586/era.09.35 (2009).

26 Sylvester, R. J., van der Meijden, A. P., Witjes, J. A. & Kurth, K. Bacillus calmette-guerin versus chemotherapy for the intravesical treatment of patients with carcinoma in situ of the bladder: a meta-analysis of the published results of randomized clinical trials. *The Journal of Urology* **174**, 86-91; discussion 91-82, doi:10.1097/01.ju.0000162059.64886.1c (2005).

27 O'Donnell, M. A. & Boehle, A. Treatment options for BCG failures. *World Journal of Urology* **24**, 481-487, doi:10.1007/s00345-006-0112-0 (2006).

28 Raj, G. V. *et al.* Treatment paradigm shift may improve survival of patients with high risk superficial bladder cancer. *The Journal of Urology* **177**, 1283-1286; discussion 1286, doi:10.1016/j.juro.2006.11.090 (2007).

29 Stein, J. P. *et al.* Radical cystectomy in the treatment of invasive bladder cancer: long-term results in 1,054 patients. *J Clin Oncol* **19**, 666-675 (2001).

30 Choudhury, A. & Cowan, R. Bladder preservation multimodality therapy as an alternative to radical cystectomy for treatment of muscle invasive bladder cancer. *BJU International* **108**, E313, doi:10.1111/j.1464-410X.2011.10672_3.x (2011).

31 Yates, D. R. & Roupret, M. Failure of bacille Calmette-Guerin in patients with high risk non-muscle-invasive bladder cancer unsuitable for radical cystectomy: an update of available treatment options. *BJU International* **106**, 162-167, doi:10.1111/j.1464-410X.2010.09272.x (2010).

32 Brooks, N. A. & O'Donnell, M. A. Treatment options in non-muscle-invasive bladder cancer after BCG failure. *Indian Journal of Urology : IJU : journal of the Urological Society of India* **31**, 312-319, doi:10.4103/0970-1591.166475 (2015).

33 Yates, D. R. *et al.* Treatment options available for bacillus Calmette-Guerin failure in non-muscle-invasive bladder cancer. *European Urology* **62**, 1088-1096, doi:10.1016/j.eururo.2012.08.055 (2012).

34 Sylvester, R. J. *et al.* Predicting recurrence and progression in individual patients with stage Ta T1 bladder cancer using EORTC risk tables: a combined analysis of 2596 patients from seven EORTC trials. *European Urology* **49**, 466-465; discussion 475-467, doi:10.1016/j.eururo.2005.12.031 (2006).

35 Dutta, S. C. *et al.* Clinical under staging of high risk nonmuscle invasive urothelial carcinoma treated with radical cystectomy. *J Urol* **166**, 490-493 (2001).

36 Herr, H. W. & Donat, S. M. Quality control in transurethral resection of bladder tumours. *BJU International* **102**, 1242-1246, doi:10.1111/j.1464-410X.2008.07966.x (2008).

37 Herr, H. W. Restaging transurethral resection of high risk superficial bladder cancer improves the initial response to bacillus Calmette-Guerin therapy. *J Urol* **174**, 2134-2137, doi:10.1097/01.ju.0000181799.81119.fc (2005).

38 Jocham, D., Stepp, H. & Waidelich, R. Photodynamic diagnosis in urology: state-of-the-art. *European Urology* **53**, 1138-1148, doi:10.1016/j.eururo.2007.11.048 (2008).

39 Power, N. E. & Izawa, J. Comparison of Guidelines on Non-Muscle Invasive Bladder Cancer (EAU, CUA, AUA, NCCN, NICE). *Bladder Cancer* **2**, 27-36, doi:10.3233/BLC-150034 (2016).

40 Agostinis, P. *et al.* Photodynamic therapy of cancer: an update. *CA Cancer J Clin* **61**, 250-281, doi:10.3322/caac.20114 (2011).

41 Bugelski, P. J., Porter, C. W. & Dougherty, T. J. Autoradiographic distribution of hematoporphyrin derivative in normal and tumor tissue of the mouse. *Cancer Research* **41**, 4606-4612 (1981).

42 Bisson, J. F., Notter, D., Labrude, P., Vigneron, C. & Guillemin, F. Induction of superficial bladder tumors in the female Fischer 344 rats with AY-27 tumor cells for the study of diffusion and localization of hemoglobin derived components (hematoporphyrin derivative) in view of photochemotherapy. *Artif Cells Blood Substit Immobil Biotechnol* **27**, 77-84 (1999).

43 Prout, G. R., Jr. *et al.* Photodynamic therapy with hematoporphyrin derivative in the treatment of superficial transitional-cell carcinoma of the bladder. *N Engl J Med* **317**, 1251-1255, doi:10.1056/NEJM198711123172003 (1987).

44 Tsuchiya, A. *et al.* Hematoporphyrin derivative and laser photoradiation in the diagnosis and treatment of bladder cancer. *The Journal of Urology* **130**, 79-82 (1983).

45 Nseyo, U. O., Shumaker, B., Klein, E. A. & Sutherland, K. Photodynamic therapy using porfimer sodium as an alternative to cystectomy in patients with refractory transitional cell carcinoma in situ of the bladder. Bladder Photofrin Study Group. *The Journal of Urology* **160**, 39-44 (1998).

46 Walther, M. M. The role of photodynamic therapy in the treatment of recurrent superficial bladder cancer. *The Urologic clinics of North America* **27**, 163-170 (2000).

47 Shulok, J. R., Klaunig, J. E., Selman, S. H., Schafer, P. J. & Goldblatt, P. J. Cellular effects of hematoporphyrin derivative photodynamic therapy on normal

and neoplastic rat bladder cells. *The American Journal of Pathology* **122**, 277-283 (1986).

48 Kelly, J. F. & Snell, M. E. Hematoporphyrin derivative: a possible aid in the diagnosis and therapy of carcinoma of the bladder. *The Journal of Urology* **115**, 150-151 (1976).

49 Jichlinski, P. & Leisinger, H. J. Photodynamic therapy in superficial bladder cancer: past, present and future. *Urological Research* **29**, 396-405 (2001).

50 Pass, H. I. Photodynamic therapy in oncology: mechanisms and clinical use. *Journal of the National Cancer Institute* **85**, 443-456 (1993).

51 D'Hallewin, M. A. & Baert, L. Long-term results of whole bladder wall photodynamic therapy for carcinoma in situ of the bladder. *Urology* **45**, 763-767, doi:10.1016/S0090-4295(99)80080-6 (1995).

52 Harty, J. I. *et al.* Complications of whole bladder dihematoporphyrin ether photodynamic therapy. *The Journal of Urology* **141**, 1341-1346 (1989).

53 Jocham, D., Baumgartner, R., Stepp, H. & Unsold, E. Clinical experience with the integral photodynamic therapy of bladder carcinoma. *Journal of Photochemistry and Photobiology. B, Biology* **6**, 183-187 (1990).

54 Pope, A. J. & Bown, S. G. Photodynamic therapy. *British Journal of Urology* **68**, 1-9 (1991).

55 Benson, R. C., Jr. *et al.* Detection and localization of In situ carcinoma of the bladder with hematoporphyrin derivative. *Mayo Clin Proc* **57**, 548-555 (1982).

56 Kelly, J. F. Haematoporphyrins in the diagnosis and treatment of carcinoma of the bladder. *Proc R Soc Med* **68**, 527-528 (1975).

57 Quint, R. H., Hett, J. H. & Wallace, F. J. Fluorescence cystoscopy. *The Journal of Urology* **95**, 208-214 (1966).

58 Baumgartner, R. *et al.* A fluorescence imaging device for endoscopic detection of early stage cancer – instrumental and experimental studies. *Photochem Photobiol* **46**, 759-763 (1987).

59 Xiao, Z., Brown, K., Tulip, J. & Moore, R. B. Whole bladder photodynamic therapy for orthotopic superficial bladder cancer in rats: a study of intravenous and intravesical administration of photosensitizers. *The Journal of Urology* **169**, 352-356, doi:10.1097/01.ju.0000039350.39402.f0 (2003).

60 Xiao, Z. *et al.* Biodistribution of Photofrin II and 5-aminolevulinic acid-induced protoporphyrin IX in normal rat bladder and bladder tumor models: implications for photodynamic therapy. *Photochemistry and Photobiology* **67**, 573-583 (1998).

61 Chang, S. C., MacRobert, A. J. & Bown, S. G. Biodistribution of protoporphyrin IX in rat urinary bladder after intravesical instillation of 5-aminolevulinic acid. *The Journal of Urology* **155**, 1744-1748 (1996).

62 Gronlund-Pakkanen, S. *et al.* The fluorescence biodistribution and kinetics of aminolevulinic acid induced protoporphyrin IX in the bladder of a rat model with orthotopic urothelial carcinoma. *The Journal of Urology* **167**, 1848-1853 (2002).

63 Fotinos, N., Campo, M. A., Popowycz, F., Gurny, R. & Lange, N. 5-Aminolevulinic acid derivatives in photomedicine: Characteristics, application and perspectives. *Photochemistry and Photobiology* **82**, 994-1015, doi:10.1562/2006-02-03-IR-794 (2006).

64 Yavari, N., Andersson-Engels, S., Segersten, U. & Malmstrom, P. U. An overview on preclinical and clinical experiences with photodynamic therapy for bladder cancer. *The Canadian Journal of Urology* **18**, 5778-5786 (2011).

65 Bader, M. J. *et al.* Photodynamic therapy of bladder cancer - a phase I study using hexaminolevulinate (HAL). *Urologic Oncology* **31**, 1178-1183, doi:10.1016/j.urolonc.2012.02.007 (2013).

66 Marti, A. *et al.* Comparison of aminolevulinic acid and hexylester aminolevulinate induced protoporphyrin IX distribution in human bladder cancer. *The Journal of Urology* **170**, 428-432, doi:10.1097/01.ju.0000075054.38441.2d (2003).

67 Burger, M. *et al.* Photodynamic diagnosis of non-muscle-invasive bladder cancer with hexaminolevulinate cystoscopy: a meta-analysis of detection and recurrence based on raw data. *European Urology* **64**, 846-854, doi:10.1016/j.eururo.2013.03.059 (2013).

68 Gakis, G. & Fahmy, O. Systematic Review and Meta-Analysis on the Impact of Hexaminolevulinate- Versus White-Light Guided Transurethral Bladder Tumor Resection on Progression in Non-Muscle Invasive Bladder Cancer. *Bladder Cancer* **2**, 293-300, doi:10.3233/BLC-160060 (2016).

69 Chang, S. S. *et al.* Diagnosis and Treatment of Non-Muscle Invasive Bladder Cancer: AUA/SUO Guideline. *The Journal of Urology* **196**, 1021-1029, doi:10.1016/j.juro.2016.06.049 (2016).

70 Mowatt, G. *et al.* Photodynamic diagnosis of bladder cancer compared with white light cystoscopy: Systematic review and meta-analysis. *International Journal of Technology Assessment in Health Care* **27**, 3-10, doi:10.1017/S0266462310001364 (2011).

71 Ray, E. R. *et al.* Hexylaminolaevulinate fluorescence cystoscopy in patients previously treated with intravesical bacille Calmette-Guerin. *BJU international* **105**, 789-794, doi:10.1111/j.1464-410X.2009.08839.x (2010).

72 Chin, W. W., Lau, W. K., Heng, P. W., Bhuvaneswari, R. & Olivo, M. Fluorescence imaging and phototoxicity effects of new formulation of chlorin e6-polyvinylpyrrolidone. *Journal of Photochemistry and Photobiology. B, Biology* **84**, 103-110, doi:10.1016/j.jphotobiol.2006.02.002 (2006).

73 Chin, W. W., Lau, W. K., Bhuvaneswari, R., Heng, P. W. & Olivo, M. Chlorin e6-polyvinylpyrrolidone as a fluorescent marker for fluorescence diagnosis of human bladder cancer implanted on the chick chorioallantoic membrane model. *Cancer Letters* **245**, 127-133, doi:10.1016/j.canlet.2005.12.041 (2007).

74 Lee, L. S. *et al.* Chlorin e6-polyvinylpyrrolidone mediated photodynamic therapy--A potential bladder sparing option for high risk non-muscle invasive bladder cancer. *Photodiagnosis and Photodynamic Therapy* **7**, 213-220, doi:10.1016/j.pdpdt.2010.08.005 (2010).

75 Bae, S. M. *et al.* Photodynamic effects of Radachlorin on cervical cancer cells. *Cancer research and treatment. Official Journal of Korean Cancer Association* **36**, 389-394, doi:10.4143/crt.2004.36.6.389 (2004).

76 Lee, J. Y. *et al.* Efficacy and safety of photodynamic therapy for recurrent, high grade nonmuscle invasive bladder cancer refractory or intolerant to bacille Calmette-Guerin immunotherapy. *The Journal of Urology* **190**, 1192-1199, doi:10.1016/j.juro.2013.04.077 (2013).

77 Cheng, L. *et al.* Tumor size predicts the survival of patients with pathologic stage T2 bladder carcinoma: a critical evaluation of the depth of muscle invasion. *Cancer* **85**, 2638-2647 (1999).

78 Kamuhabwa, A. A. *et al.* Biodistribution of hypericin in orthotopic transitional cell carcinoma bladder tumors: implication for whole bladder wall photodynamic therapy. *Int J Cancer* **97**, 253-260 (2002).

79 Kamuhabwa, A. A. *et al.* Whole bladder wall photodynamic therapy of transitional cell carcinoma rat bladder tumors using intravesically administered hypericin. *Int J Cancer* **107**, 460-467, doi:10.1002/ijc.11396 (2003).

80 Kubin, A. *et al.* Fluorescence diagnosis of bladder cancer with new water soluble hypericin bound to polyvinylpyrrolidone: PVP-hypericin. *Photochem Photobiol* **84**, 1560-1563, doi:10.1111/j.1751-1097.2008.00384.x (2008).

81 Sim, H. G., Lau, W. K., Olivo, M., Tan, P. H. & Cheng, C. W. Is photodynamic diagnosis using hypericin better than white-light cystoscopy for detecting superficial bladder carcinoma? *BJU International* **95**, 1215-1218, doi:10.1111/j.1464-410X.2005.05508.x (2005).

82 D'Hallewin, M. A., Kamuhabwa, A. R., Roskams, T., De Witte, P. A. & Baert, L. Hypericin-based fluorescence diagnosis of bladder carcinoma. *BJU International* **89**, 760-763 (2002).

83 D'Hallewin, M. A., De Witte, P. A., Waelkens, E., Merlevede, W. & Baert, L. Fluorescence detection of flat bladder carcinoma in situ after intravesical instillation of hypericin. *The Journal of Urology* **164**, 349-351 (2000).

84 Straub, M., Russ, D., Horn, T., Gschwend, J. E. & Abrahamsberg, C. A phase IIA dose-finding study of PVP-hypericin fluorescence cystoscopy for detection of nonmuscle-invasive bladder cancer. *Journal of Endourology / Endourological Society* **29**, 216-222, doi:10.1089/end.2014.0282 (2015).

85 Stenzl, A. *et al.* Detection and clinical outcome of urinary bladder cancer with 5-aminolevulinic acid-induced fluorescence cystoscopy : A multicenter randomized, double-blind, placebo-controlled trial. *Cancer* **117**, 938-947, doi:10.1002/cncr.25523 (2011).

86 Schumacher, M. C. *et al.* Transurethral resection of non-muscle-invasive bladder transitional cell cancers with or without 5-aminolevulinic Acid under visible and fluorescent light: results of a prospective, randomised, multicentre study. *European Urology* **57**, 293-299, doi:10.1016/j.eururo.2009.10.030 (2010).

87 Francois, A. *et al.* How to avoid local side effects of bladder photodynamic therapy: impact of the fluence rate. *The Journal of Urology* **190**, 731-736, doi:10.1016/j.juro.2013.01.046 (2013).

88 Jichlinski, P. Photodynamic applications in superficial bladder cancer: facts and hopes! *Journal of environmental pathology, toxicology and oncology : official organ of the International Society for Environmental Toxicology and Cancer* **25**, 441-451 (2006).

89 Seidl, J. *et al.* Optimization of differential photodynamic effectiveness between normal and tumor urothelial cells using 5-aminolevulinic acid-induced protoporphyrin IX as sensitizer. *Int J Cancer* **92**, 671-677 (2001).

90 Lin, T. Y. *et al.* Novel theranostic nanoporphyrins for photodynamic diagnosis and trimodal therapy for bladder cancer. *Biomaterials* **104**, 339-351, doi:10.1016/j.biomaterials.2016.07.026 (2016).

91 Ellsworth, R. E. *et al.* Amplification of HER2 is a marker for global genomic instability. *BMC Cancer* **8**, 297, doi:10.1186/1471-2407-8-297 (2008).

92 Wadhwa, N., Mathew, B. B., Jatawa, S. K. & Tiwari, A. Genetic instability in urinary bladder cancer: An evolving hallmark. *J Postgrad Med* **59**, 284-288, doi:10.4103/0022-3859.123156 (2013).

93 Bonberg, N. *et al.* Chromosomal instability and bladder cancer: the UroVysion(TM) test in the UroScreen study. *BJU International* **112**, E372-382, doi:10.1111/j.1464-410X.2012.11666.x (2013).

94 Kawamura, K. *et al.* Centrosome hyperamplification and chromosomal instability in bladder cancer. *European Urology* **43**, 505-515 (2003).

95 Slamon, D. J. *et al.* Studies of the HER-2/neu proto-oncogene in human breast and ovarian cancer. *Science* **244**, 707-712 (1989).

96 Brown, J. L., Russell, P. J., Philips, J., Wotherspoon, J. & Raghavan, D. Clonal analysis of a bladder cancer cell line: an experimental model of tumour heterogeneity. *British Journal of Cancer* **61**, 369-376 (1990).

97 Russell, P. J. *et al.* Establishment and characterization of a new human bladder cancer cell line showing features of squamous and glandular differentiation. *International Journal of Cancer. Journal International du Cancer* **41**, 74-82 (1988).

98 Perou, C. M. *et al.* Molecular portraits of human breast tumours. *Nature* **406**, 747-752, doi:10.1038/35021093 (2000).

99 Hemmings, B. A. Akt signaling: linking membrane events to life and death decisions. *Science* **275**, 628-630 (1997).

100 Xie, J., Lee, S. & Chen, X. Nanoparticle-based theranostic agents. *Adv Drug Deliv Rev* **62**, 1064-1079, doi:10.1016/j.addr.2010.07.009 (2010).

101 Polikarpov, D. *et al.* Mossbauer study of exogenous iron redistribution between the brain and the liver after administration of (Fe3O4)-Fe-57 ferrofluid in the ventricle of the rat brain. *J Magn Magn Mater* **380**, 78-84, doi:10.1016/j.jmmm.2014.10.084 (2015).

102 Polikarpov, D. *et al.* Mossbauer evidence of (Fe3O4)-Fe-57 based ferrofluid biodegradation in the brain. *Hyperfine Interact* **226**, 421-430, doi:10.1007/s10751-013-1002-7 (2014).

103 Polikarpov, D. M. *et al.* Efficiency analysis of clearance of two types of exogenous iron from the rat brain by Mossbauer spectroscopy. *Hyperfine Interact* **218**, 83-88, doi:10.1007/s10751-012-0713-5 (2013).

104 McCarthy, J. R. & Weissleder, R. Multifunctional magnetic nanoparticles for targeted imaging and therapy. *Advanced Drug Delivery Reviews* **60**, 1241-1251, doi:10.1016/j.addr.2008.03.014 (2008).

105 Kelkar, S. S. & Reineke, T. M. Theranostics: Combining Imaging and Therapy. *Bioconjugate Chem* **22**, 1879-1903, doi:10.1021/bc200151q (2011).

106 Zhang, Z. J. *et al.* Mesoporous Silica-Coated Gold Nanorods as a Light-Mediated Multifunctional Theranostic Platform for Cancer Treatment. *Adv Mater* **24**, 1418-1423, doi:10.1002/adma.201104714 (2012).

107 Wang, Y. *et al.* Mesoporous silica nanoparticles in drug delivery and biomedical applications. *Nanomed-Nanotechnol* **11**, 313-327, doi:10.1016/j.nano.2014.09.014 (2015).

108 Li, Z. X., Barnes, J. C., Bosoy, A., Stoddart, J. F. & Zink, J. I. Mesoporous silica nanoparticles in biomedical applications. *Chem Soc Rev* **41**, 2590-2605, doi:10.1039/c1cs15246g (2012).

109 Nuiachristos, V. Fluorescence molecular imaging. *Annu Rev Biomed Eng* **8**, 1-33, doi:10.1146/annurev.bioeng.8.061505.095831 (2006).

110 Liu, Q., Feng, W., Yang, T., Yi, T. & Li, F. Upconversion luminescence imaging of cells and small animals. *Nature Protocols* **8**, 2033-2044, doi:10.1038/nprot.2013.114 (2013).

111 le Masne de Chermont, Q. *et al.* Nanoprobes with near-infrared persistent luminescence for in vivo imaging. *Proceedings of the National Academy of Sciences of the United States of America* **104**, 9266-9271, doi:10.1073/pnas.0702427104 (2007).

112 Schenke-Layland, K., Riemann, I., Damour, O., Stock, U. A. & Konig, K. Two-photon microscopes and in vivo multiphoton tomographs--powerful diagnostic tools for tissue engineering and drug delivery. *Advanced Drug Delivery Reviews* **58**, 878-896, doi:10.1016/j.addr.2006.07.004 (2006).

113 Frangioni, J. V. In vivo near-infrared fluorescence imaging. *Current Opinion in Chemical Biology* **7**, 626-634 (2003).

114 Smith, A. M., Mancini, M. C. & Nie, S. M. BIOIMAGING Second window for in vivo imaging. *Nat Nanotechnol* **4**, 710-711, doi:10.1038/nnano.2009.326 (2009).

115 Weissleder, R. A clearer vision for in vivo imaging. *Nat Biotechnol* **19**, 316-317, doi:Doi 10.1038/86684 (2001).

116 Li, Z. Q., Zhang, Y. & Jiang, S. Multicolor Core/Shell-Structured Upconversion Fluorescent Nanoparticles (vol 20, pg 4765, 2008). *Adv Mater* **21**, 4768-4768, doi:10.1002/adma.200801056 (2009).

117 Suyver, J. F., Grimm, J., Kramer, K. W. & Gudel, H. U. Highly efficient near-infrared to visible up-conversion process in NaYF4 : Er,3+Yb3+. *J Lumin* **114**, 53-59, doi:10.1016/j.jlumin.2004.11.012 (2005).

118 Kramer, K. W. *et al.* Hexagonal sodium yttrium fluoride based green and blue emitting upconversion phosphors. *Chem Mater* **16**, 1244-1251, doi:10.1021/cm031124o (2004).

119 Li, P., Peng, Q. & Li, Y. D. Dual-Mode Luminescent Colloidal Spheres from Monodisperse Rare-Earth Fluoride Nanocrystals. *Adv Mater* **21**, 1945-1948, doi:10.1002/adma.200803228 (2009).

120 Palmer, R. J., Butenhoff, J. L. & Stevens, J. B. Cytotoxicity of the rare earth metals cerium, lanthanum, and neodymium in vitro: comparisons with cadmium in a

pulmonary macrophage primary culture system. *Environmental Research* **43**, 142-156 (1987).

121 Zhou, J. C. *et al.* Bioimaging and toxicity assessments of near-infrared upconversion luminescent NaYF4:Yb,Tm nanocrystals. *Biomaterials* **32**, 9059-9067, doi:10.1016/j.biomaterials.2011.08.038 (2011).

122 Nadort, A. *et al.* Quantitative imaging of single upconversion nanoparticles in biological tissue. *PloS one* **8**, e63292, doi:10.1371/journal.pone.0063292 (2013).

123 Maeda, H. Tumor-selective delivery of macromolecular drugs via the EPR effect: background and future prospects. *Bioconjugate Chemistry* **21**, 797-802, doi:10.1021/bc100070g (2010).

124 Fan, W. P. *et al.* A smart upconversion-based mesoporous silica nanotheranostic system for synergetic chemo-/radio-/photodynamic therapy and simultaneous MR/UCL imaging. *Biomaterials* **35**, 8992-9002, doi:10.1016/j.biomaterials.2014.07.024 (2014).

125 Qiao, X. F. *et al.* Triple-functional core-shell structured upconversion luminescent nanoparticles covalently grafted with photosensitizer for luminescent, magnetic resonance imaging and photodynamic therapy in vitro. *Nanoscale* **4**, 4611-4623, doi:10.1039/c2nr30938f (2012).

126 Liang, X. H. *et al.* A novel template-free and one-step method to fabricate hollow mesoporous structured upconversion luminescent NaYF4: Yb3+, Er3+ nanoparticles. *Mater Lett* **129**, 107-110, doi:10.1016/j.matlet.2014.05.049 (2014).

127 Zhou, A. G., Wei, Y. C., Wu, B. Y., Chen, Q. & Xing, D. Pyropheophorbide A and c(RGDyK) Comodified Chitosan-Wrapped Upconversion Nanoparticle for Targeted Near-Infrared Photodynamic Therapy. *Mol Pharmaceut* **9**, 1580-1589, doi:10.1021/mp200590y (2012).

128 Liu, K. *et al.* Covalently Assembled NIR Nanoplatform for Simultaneous Fluorescence Imaging and Photodynamic Therapy of Cancer Cells. *Acs Nano* **6**, 4054-4062, doi:10.1021/nn300436b (2012).

129 Zeng, L. Y. *et al.* In vivo targeted magnetic resonance imaging and visualized photodynamic therapy in deep-tissue cancers using folic acid-functionalized superparamagnetic-upconversion nanocomposites. *Nanoscale* **7**, 8946-8954, doi:10.1039/c5nr01932j (2015).

130 Cui, S. S. *et al.* In Vivo Targeted Deep-Tissue Photodynamic Therapy Based on Near-Infrared Light Triggered Upconversion Nanoconstruct. *Acs Nano* **7**, 676-688, doi:10.1021/nn304872n (2013).

131 Zhang, P., Steelant, W., Kumar, M. & Scholfield, M. Versatile photosensitizers for photodynamic therapy at infrared excitation. *J Am Chem Soc* **129**, 4526-+, doi:10.1021/ja0700707 (2007).

132 Care, A., Bergquist, P. L. & Sunna, A. Solid-binding peptides: smart tools for nanobiotechnology. *Trends Biotechnol* **33**, 259-268, doi:10.1016/j.tibtech.2015.02.005 (2015).

133 Avvakumova, S., Colombo, M., Tortora, P. & Prosperi, D. Biotechnological approaches toward nanoparticle biofunctionalization. *Trends Biotechnol* **32**, 11-20, doi:10.1016/j.tibtech.2013.09.006 (2014).

134 Sapsford, K. E. *et al.* Functionalizing Nanoparticles with Biological Molecules: Developing Chemistries that Facilitate Nanotechnology. *Chem Rev* **113**, 1904-2074, doi:10.1021/cr300143v (2013).

135 Camarero, J. A. Recent developments in the site-specific immobilization of proteins onto solid supports. *Biopolymers* **90**, 450-458, doi:10.1002/bip.20803 (2008).

136 Sunna, A., Chi, F. & Bergquist, P. L. A linker peptide with high affinity towards silica-containing materials. *New Biotechnol* **30**, 485-492, doi:10.1016/j.nbt.2012.11.022 (2013).

137 Liang, L. E. *et al.* Facile Assembly of Functional Upconversion Nanoparticles for Targeted Cancer Imaging and Photodynamic Therapy. *Acs Appl Mater Inter* **8**, 11945-11953, doi:10.1021/acsami.6b00713 (2016).

138 Gnanasammandhan, M. K., Idris, N. M., Bansal, A., Huang, K. & Zhang, Y. Near-IR photoactivation using mesoporous silica-coated NaYF4:Yb,Er/Tm upconversion nanoparticles. *Nat Protoc* **11**, 688-713, doi:10.1038/nprot.2016.035 (2016).

139 Xu, F. *et al.* Mesoporous-silica-coated upconversion nanoparticles loaded with vitamin B-12 for near-infrared-light mediated photodynamic therapy. *Mater Lett* **167**, 205-208, doi:10.1016/j.matlet.2015.12.105 (2016).

140 Liu, J. N., Bu, W. B. & Shi, J. L. Silica Coated Upconversion Nanoparticles: A Versatile Platform for the Development of Efficient Theranostics. *Accounts Chem Res* **48**, 1797-1805, doi:10.1021/acs.accounts.5b00078 (2015).

141 Lai, J. P., Shah, B. R., Zhang, Y. X., Yang, L. T. & Lee, K. B. Real-Time Monitoring of ATP-Responsive Drug Release Using Mesoporous-Silica-Coated Multicolor Upconversion Nanoparticles. *Acs Nano* **9**, 5234-5245, doi:10.1021/acsnano.5b00641 (2015).

142 Jayakumar, M. K. G., Bansal, A., Li, B. N. & Zhang, Y. Mesoporous silica-coated upconversion nanocrystals for near infrared light-triggered control of gene expression in zebrafish. *Nanomedicine-Uk* **10**, 1051-1061, doi:10.2217/Nnm.14.198 (2015).

143 Bhattacharjee, S. DLS and zeta potential - What they are and what they are not? *Journal of controlled release : official journal of the Controlled Release Society* **235**, 337-351, doi:10.1016/j.jconrel.2016.06.017 (2016).

144 Care, A., Chi, F., Bergquist, P. L. & Sunna, A. Biofunctionalization of silica-coated magnetic particles mediated by a peptide. *J Nanopart Res* **16**, doi:ARTN 254310.1007/s11051-014-2543-7 (2014).

145 Coyle, B. L. & Baneyx, F. A Cleavable Silica-Binding Affinity Tag for Rapid and Inexpensive Protein Purification. *Biotechnol Bioeng* **111**, 2019-2026, doi:10.1002/bit.25257 (2014).

146 Akerstrom, B. & Bjorck, L. A Physicochemical Study of Protein-G, a Molecule with Unique Immunoglobulin-G-Binding Properties. *J Biol Chem* **261**, 240-247 (1986).

147 Akerstrom, B., Brodin, T., Reis, K. & Bjorck, L. Protein-G - a Powerful Tool for Binding and Detection of Monoclonal and Polyclonal Antibodies. *J Immunol* **135**, 2589-2592 (1985).

148 Walker, K. Z., Russell, P. J., Kingsley, E. A., Philips, J. & Raghavan, D. Detection of Malignant-Cells in Voided Urine from Patients with Bladder-Cancer, a Novel Monoclonal Assay. *J Urology* **142**, 1578-1583 (1989).

149 Russell, P. J. *et al.* Establishment and Characterization of a New Human Bladder-Cancer Cell-Line Showing Features of Squamous and Glandular Differentiation. *Int J Cancer* **41**, 74-82, doi:DOI 10.1002/ijc.2910410115 (1988).

150 Truong, Q. *et al.* Glypican-1 as a Biomarker for Prostate Cancer: Isolation and Characterization. *J Cancer* **7**, 1002-1009, doi:10.7150/jca.14645 (2016).

151 Yeh, M. C. *et al.* Glypican-1: a new biomarker for the detection of prostate cancer. *Bju Int* **118**, 27-27 (2016).

152 Filmus, J. & Selleck, S. B. Glypicans: proteoglycans with a surprise. *J Clin Invest* **108**, 497-501, doi:10.1172/JCI13712 (2001).

153 Perrimon, N. & Bernfield, M. Specificities of heparan sulphate proteoglycans in developmental processes. *Nature* **404**, 725-728, doi:10.1038/35008000 (2000).

154 Jeet, V. *et al.* More than a biomarker: exploring the role of glypican-1 as a new therapeutic target for prostate cancer. *Bju Int* **118**, 28-28 (2016).

155 Sabanathan, D. *et al.* MILGa-01-a first in human study assessing the safety and tolerability of chMIL38 in prostate cancer. *Bju Int* **118**, 14-15 (2016).

156 Shore, N. *et al.* Glypican-1 as a Biomarker for Prostate Cancer. *J Urology* **193**, E496-E496 (2015).

157 Diamandis, E. P. & Plebani, M. Glypican-1 as a highly sensitive and specific pancreatic cancer biomarker. *Clin Chem Lab Med* **54**, e1-2, doi:10.1515/cclm-2015-0773 (2016).

158 Melo, S. A. *et al.* Glypican-1 identifies cancer exosomes and detects early pancreatic cancer. *Nature* **523**, 177-182, doi:10.1038/nature14581 (2015).

159 Kayed, H. *et al.* Correlation of glypican-1 expression with TGF-beta, BMP, and activin receptors in pancreatic ductal adenocarcinoma. *Int J Oncol* **29**, 1139-1148 (2006).

160 Kleeff, J. *et al.* The cell-surface heparan sulfate proteoglycan glypican-1 regulates growth factor action in pancreatic carcinoma cells and is overexpressed in human pancreatic cancer. *J Clin Invest* **102**, 1662-1673, doi:10.1172/JCI4105 (1998).

161 Hara, H. *et al.* Overexpression of glypican-1 implicates poor prognosis and their chemoresistance in oesophageal squamous cell carcinoma. *Br J Cancer* **115**, 66-75, doi:10.1038/bjc.2016.183 (2016).

162 Matsuda, K. *et al.* Glypican-1 is overexpressed in human breast cancer and modulates the mitogenic effects of multiple heparin-binding growth factors in breast cancer cells. *Cancer Res* **61**, 5562-5569 (2001).

163 Su, G. *et al.* Glypican-1 is frequently overexpressed in human gliomas and enhances FGF-2 signaling in glioma cells. *Am J Pathol* **168**, 2014-2026, doi:10.2353/ajpath.2006.050800 (2006).

164 Qiao, D., Meyer, K., Mundhenke, C., Drew, S. A. & Friedl, A. Heparan sulfate proteoglycans as regulators of fibroblast growth factor-2 signaling in brain endothelial cells. Specific role for glypican-1 in glioma angiogenesis. *J Biol Chem* **278**, 16045-16053, doi:10.1074/jbc.M211259200 (2003).

165 Xing, H. *et al.* Multifunctional nanoprobes for upconversion fluorescence, MR and CT trimodal imaging. *Biomaterials* **33**, 1079-1089, doi:10.1016/j.biomaterials.2011.10.039 (2012).

166 Ansari, A. A., Yadav, R. & Rai, S. B. Influence of surface coating on structural, morphological and optical properties of upconversion-luminescent LaF3:Yb/Er nanoparticles. *Appl Phys a-Mater* **122**, doi:ARTN 63510.1007/s00339-016-0160-2 (2016).

167 Russell, P. J. *et al.* Immunohistochemical characterisation of the monoclonal antibody BLCA-38 for the detection of prostate cancer. *Cancer Immunol Immun* **53**, 995-1004, doi:10.1007/s00262-004-0527-7 (2004).

168 Bubenik, J. *et al.* Established cell line of urinary bladder carcinoma (T24) containing tumour-specific antigen. *International Journal of Cancer. Journal International du Cancer* **11**, 765-773 (1973).

169 Steeg, P. S. Targeting metastasis. *Nat Rev Cancer* **16**, 201-218, doi:10.1038/nrc.2016.25 (2016).

170 Matsumura, Y. & Maeda, H. A new concept for macromolecular therapeutics in cancer chemotherapy: mechanism of tumoritropic accumulation of proteins and the antitumor agent smancs. *Cancer Res* **46**, 6387-6392 (1986).

171 Bazak, R., Houri, M., Achy, S. E., Hussein, W. & Refaat, T. Passive targeting of nanoparticles to cancer: A comprehensive review of the literature. *Mol Clin Oncol* **2**, 904-908, doi:10.3892/mco.2014.356 (2014).

172 Bazak, R., Houri, M., El Achy, S., Kamel, S. & Refaat, T. Cancer active targeting by nanoparticles: a comprehensive review of literature. *J Cancer Res Clin Oncol* **141**, 769-784, doi:10.1007/s00432-014-1767-3 (2015).

173 Steinhauser, I., Spankuch, B., Strebhardt, K. & Langer, K. Trastuzumab-modified nanoparticles: optimisation of preparation and uptake in cancer cells. *Biomaterials* **27**, 4975-4983, doi:10.1016/j.biomaterials.2006.05.016 (2006).

174 Gnanasammandhan, M. K., Idris, N. M., Bansal, A., Huang, K. & Zhang, Y. Near-IR photoactivation using mesoporous silica-coated NaYF4:Yb,Er/Tm upconversion nanoparticles. *Nat Protoc* **11**, 688-713, doi:10.1038/nprot.2016.035 (2016).

175 Liu, J. N., Bu, W. B. & Shi, J. L. Silica coated upconversion nanoparticles: a versatile platform for the development of efficient theranostics. *Acc Chem Res* **48**, 1797-1805, doi:10.1021/acs.accounts.5b00078 (2015).

176 Idris, N. M. *et al.* In vivo photodynamic therapy using upconversion nanoparticles as remote-controlled nanotransducers. *Nat Med* **18**, 1580-1585, doi:10.1038/nm.2933 (2012).

177 Cheng, L. *et al.* Multifunctional nanoparticles for upconversion luminescence/MR multimodal imaging and magnetically targeted photothermal therapy. *Biomaterials* **33**, 2215-2222, doi:10.1016/j.biomaterials.2011.11.069 (2012).

178 Zhu, X. *et al.* Temperature-feedback upconversion nanocomposite for accurate photothermal therapy at facile temperature. *Nat Commun* **7**, 10437, doi:10.1038/ncomms10437 (2016).

179 Chen, Q. *et al.* Protein modified upconversion nanoparticles for imaging-guided combined photothermal and photodynamic therapy. *Biomaterials* **35**, 2915-2923, doi:10.1016/j.biomaterials.2013.12.046 (2014).

180 Bagwe, R. P., Hilliard, L. R. & Tan, W. Surface modification of silica nanoparticles to reduce aggregation and nonspecific binding. *Langmuir* **22**, 4357-4362, doi:10.1021/la052797j (2006).